ELSEVIER

Chemical Geology 225 (2006) 91–120

CHEMICAL GEOLOGY
INCLUDING
ISOTOPE GEOSCIENCE

www.elsevier.com/locate/chemgeo

Interpretation of (U–Th)/He single grain ages from slowly cooled crustal terranes: A case study from the Transantarctic Mountains of southern Victoria Land

P.G. Fitzgerald *, S.L. Baldwin, L.E. Webb, P.B O'Sullivan [1]

Department of Earth Sciences, Syracuse University, Syracuse, NY 13244, USA

Received 8 April 2005; received in revised form 5 September 2005; accepted 19 September 2005

Abstract

Low temperature thermochronologic techniques (e.g. apatite fission track (AFT) thermochronology and (U–Th)/He dating) constrain near-surface *T–t* paths and are often applied to uplift/denudation and landscape evolution studies. Samples collected in vertical profiles from granitic walls on either side of the Ferrar Glacier, southern Victoria Land, Antarctica were analyzed using AFT thermochronology and apatite (U–Th)/He dating to further constrain the lowest temperature thermal history of this portion of the Transantarctic Mountains. AFT central ages vary systematically with elevation and together with track length information define a multi-stage cooling/denudation history in the Cretaceous and early Tertiary. Apatite (U–Th)/He single grain age variation with elevation is not as systematic with considerable intra-sample age variation. Although many complicating factors (e.g., U- and Th-rich (micro)inclusions, fluid inclusions, variation in crystal size, α-particle ejection correction, zonation and α-particle ejection correction, implantation of He into a crystal or impediment of He diffusion out of a crystal, and ^{147}Sm-derived α-particles) may contribute to age dispersion, we found that variation in single grain ages correlated with cooling rate. Samples that cooled relatively quickly have less variation in single grain ages, whereas samples that cooled relatively slowly (<3 °C/m.y.) or resided within an (U–Th)/He partial retention zone (HePRZ) prior to more rapid cooling have a comparatively greater variation in ages.

Decay of U and Th via α-particle emission creates a ^{4}He concentration profile dependent upon the initial parent [U,Th] within a crystal. Variation of single grain ages for samples with non-homogeneous [U,Th] distributions will be enhanced with long residence time in the partial retention zone (i.e., slow cooling) because of the relative importance of loss via volume diffusion and loss via α-particle ejection with respect to the [U,Th] zonation and the grain boundary. Correction of ages for α-particle ejection (F_T correction factor) typically assumes uniform U and Th distribution within the crystal and when applied to a population of crystals with different U and Th distributions will enhance the variation in ages. Most complicating factors (listed above) for apatite (U–Th)/He ages result in ages that are "too old". We propose that if considerable variation in (U–Th)/He single grain ages exists, that a weighted mean age is determined once outlier single crystal ages are excluded using the criterion of Chauvenet or a similar approach. We suggest that the "true age" or most representative age for that age population lies between the minimum (U–Th)/He age and the weighted mean age. We apply this approach, coupled with composite age profiles to better constrain the *T–t* history of the profiles along the Ferrar Glacier. Significant intra-sample variation in single crystal apatite (U–Th)/He ages and other minerals

* Corresponding author. Fax: +1 315 443 3363.

E-mail addresses: pgfitzge@syr.edu (P.G. Fitzgerald), sbaldwin@syr.edu (S.L. Baldwin), lewebb@syr.edu (L.E. Webb), osullivan@apatite.com (P.B. O'Sullivan).

[1] Now at: Apatite to Zircon, Inc., 1521 Pine Cone Rd, Moscow, ID 83843, USA.

0009-2541/$ - see front matter
doi:10.1016/j.chemgeo.2005.09.001

dated by the (U–Th)/He method should be expected, especially when the cooling rate is slow. The variation of (U–Th)/He single crystal ages is therefore another parameter that can be used to constrain low-temperature thermal histories.

Keywords: Thermochronology; (U–Th)/He dating; Apatite fission track; Transantarctic mountains

1. Introduction

Low temperature thermochronologic techniques such as apatite fission track (AFT) thermochronology and (U–Th)/He dating can provide powerful constraints on near-surface temperature–time (*T–t*) histories of rocks. These methods are commonly used to constrain the timing, amounts and rate of cooling/denudation associated with mountain building, crustal deformation, extensional tectonics and landscape evolution (e.g., Brown et al., 1994; Fitzgerald et al., 1995; Gallagher et al., 1998; Farley, 2002; Ehlers et al., 2003; Stockli et al., 2003). Combining multiple thermochronologic methods obviously allows for a more complete *T–t* history covering a greater temperature range and hence a greater range of crustal depths. As shown in other studies (e.g., Stockli et al., 2000, 2003; Armstrong et al., 2003; Reiners et al., 2003) confidence in the interpretation of a (U–Th)/He data set is strongly augmented (and vice versa) if AFT thermochronology is undertaken on the same samples.

In this study, we applied AFT thermochronology and apatite (U–Th)/He dating to a series of vertical profiles collected in basement rock across the Transantarctic Mountains (TAM) in southern Victoria Land. Our goal was to better constrain the denudation history and landscape evolution of the TAM. The TAM define the western flank of the West Antarctic rift system (WARS); a rift-system comparable in size to the Basin and Range Province (Fitzgerald et al., 1986; Tessensohn and Wörner, 1991). The TAM, >2500 km in length, are somewhat unique amongst rift-flank mountains due to their anomalously high elevations (>4000 m). Understanding the tectonic evolution of the TAM is therefore important in constraining how this range formed and the tectonic evolution of the largely ice-covered WARS. This is regionally important as the oldest sediments cored in the basin adjacent to the TAM are latest Eocene (Wilson et al., 1998; Florindo et al., 2001) whereas the rift system initially formed in the mid-Mesozoic (e.g., Elliot and Fleming, 2004). Constraining the timing and rate of denudation of the TAM and using this information to better understand their tectonic evolution, as well as that of the WARS has benefited from extensive AFT thermochronology along the TAM (Fitzgerald, 2002, and references therein). This approach has delineated episodes of denudation in the Early Cretaceous and Late Cretaceous, but the most pronounced episode documented along the TAM was initiated in the Eocene.

In this paper we present data from two vertical profiles: Peak 1880 from the southern wall of the Kukri Hills on the north side of the Ferrar Glacier and Cathedral Rocks from the south side of this glacier (Figs. 1 and 2). Both profiles were collected from the Bonney pluton, an undeformed hornblende–biotite granodiorite (Allibone et al., 1993). The AFT central ages from these profiles show good correlation with elevation; however, the (U–Th)/He data displayed considerable variation in single crystal ages for some sam-

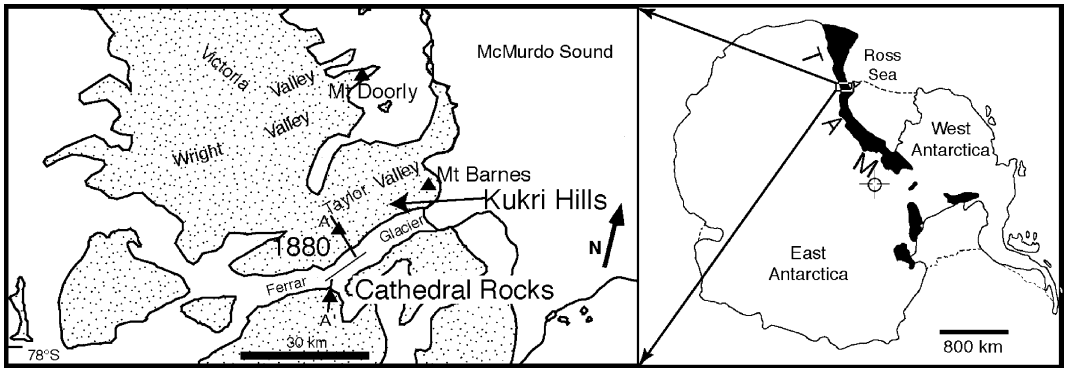

Fig. 1. Simplified map of southern Victoria Land showing localities. Stipled area = ice free areas. TAM = Transantarctic Mountains. Location of Fig. 2 A–A′ cross-section is marked.

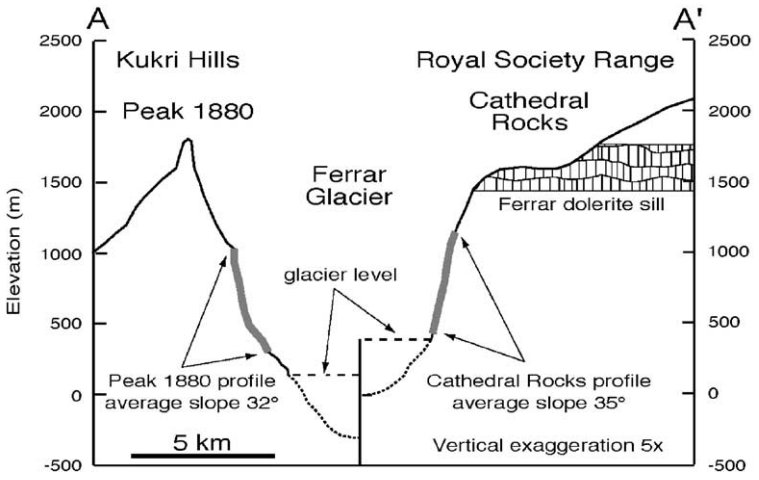

Fig. 2. North–south cross through the Ferrar Glacier showing the wavelength (λ) of topography as ~12 km and the location of the two vertical profiles (marked by thick grey lines). Topography is from the USGS 1:250,000 scale topographic map. Sub-glacial topography (dotted line) is estimated from radio-echo sounding profiles along the Ferrar Glacier (Calkin, 1974). Note the cross-section line through the two profiles are offset along the Ferrar Glacier (see Fig. 1); hence, the different glacier elevations (dashed line).

ples. Our objective in this paper is to document and explain the intra-sample variation in apatite (U–Th)/He single crystal ages. Replicate (U–Th)/He age determinations, AFT data for all samples, and the vertical profile sampling strategy provide a framework in which to interpret the age variation. We discuss possible causes for age dispersion, including the presence of U- and Th-rich (micro)inclusions, fluid inclusions, the effect of crystal size, non-homogeneous distribution of U and Th, the age-correction for α-particle ejection, external implantation of α-particles, impediment of He diffusion from a crystal, the contribution of radiogenic helium from ^{147}Sm, and modification of the He concentration profile within a crystal due to diffusion when samples are slowly cooled or resident in a He partial retention zone. Most of these effects are manifested as a variation in (U–Th)/He single grain ages. While other papers have explained and discussed these effects from a theoretical standpoint (Meesters and Dunai, 2002b; Ehlers and Farley, 2003), we discuss the practical aspects of data interpretation for samples that yield a significant variation of single crystal (U–Th)/He apatite ages. The AFT age and length data from the same samples is crucial to our interpretation of the (U–Th)/He data as the AFT thermochronology provides independent constraints on the low-temperature *T–t* history. The AFT and (U–Th)/He data are used to explain the landscape evolution of the TAM elsewhere (Fitzgerald et al., in preparation). Herein, we provide a framework within which one can interpret the intra-sample variation in apatite single grain (U–Th)/He ages from slowly cooled terranes.

2. Techniques and results

2.1. Apatite fission track thermochronology

Fission track thermochronology is based on the decay of ^{238}U via spontaneous fission that results in the formation of a linear damage zone or fission track. The density of fission tracks in a crystal is dominantly a function of the [^{238}U] and time over which tracks have accumulated, and the length of confined fission tracks is proportional to the maximum temperature each track has experienced (e.g., Green et al., 1986). Closure temperature varies with cooling rate (Dodson, 1973) and also chemical composition (e.g., Green et al., 1986). The closure temperature for an apatite crystal similar in composition to Durango apatite (0.4 wt.% Cl) that cools at 5 °C/m.y. is ~108 °C (e.g., Brandon et al., 1998). In this study, we use a closure temperature of ~100 °C for the AFT closure temperature because the Dpar (diameter of etched spontaneous fission tracks measured parallel to the *c*-axis) are very low, with a range from 1.3 to 1.6 μm (Table 1). Dpar values are representative of the kinetics of annealing of fission tracks (Carlson et al., 1999; Ketcham et al., 1999) and chemical composition (Burtner et al., 1994). For reference, the Dpar for Durango apatite, etched and measured under the same conditions as the apatite crystals from Antarctica is 2.2 μm. Fission tracks in apatite anneal at increasing rates over a range in temperatures from ~60 °C to ~110 °C (dependent on apatite chemistry), known as the partial annealing zone (PAZ). The PAZ is clearly revealed in downhole

Table 1
Apatite fission track analytical results: Peak 1880 and Cathedral Rocks, Ferrar Glacier, southern Victoria Land

Sample number	Location: latitude/longitude	Elevation (m)	No. of grains	Standard track density ($\times 10^6$ cm^{-2})	Fossil track density ($\times 10^6$ cm^{-2})	Induced track density ($\times 10^6$ cm^{-2})	χ^2 probability (%)	Central age $\pm 1\sigma$ (Ma)	Relative error (%)	[U] (ppm)	Confined tracks (mean length $\pm$ S.D. (N); μm)	Dpar (mean $\pm$ S.D.; μm)
Peak 1880 profile: southern flank of Peak 1880												
R22615	162°50.08′E	1054	20	1.62	1.079	4.689	73	65.6 ± 3.3	0.02	36	12.8 ± 0.2	1.51 ± 0.02
	77°44.65′S			(3542)	(561)	(2439)					2.4 (100)	0.20
R22616	162°50.34′E	947	20	1.25	2.296	9.224	<1	55.3 ± 3.2	15	91	12.8 ± 0.2	1.37 ± 0.02
	77°44.78′S			(2188)	(855)	(3435)					2.1 (104)	0.18
R22617	162°50.47′E	847	20	1.25	1.221	4.362	1	61.8 ± 4.6	18	43	13.0 ± 0.2	1.40 ± 0.02
	77°44.90′S			(2188)	(428)	(1529)					2.3 (101)	0.24
R22618	162°50.59′E	731	20	1.25	0.872	3.685	<1	52.9 ± 4.5	22	36	13.3 ± 0.2	1.46 ± 0.02
	77°44.98′S			(2188)	(325)	(1373)					2.2 (100)	0.21
R22619	162°50.85′E	636	25	1.43	1.910	8.073	10	59.6 ± 2.1	0	69	13.8 ± 0.2	1.55 ± 0.02
	77°45.11′S			(10028)	(1056)	(4463)					1.8 (103)	0.20
R22620	162°51.10′E	521	20	1.25	1.994	7.856	54	55.9 ± 2.3	0	77	13.2 ± 0.2	1.41 ± 0.02
	77°45.22′S			(2188)	(1013)	(3990)					2.3 (100)	0.19
R22621	162°51.10′E	413	20	1.25	1.517	6.125	7	54.4 ± 2.8	7	60	13.4 ± 0.2	1.45 ± 0.02
	77°45.24′S			(2188)	(639)	(2581)					2.1 (101)	0.21
R22622	162°51.36′E	299	14	1.36	1.067	7.904	0	43.3 ± 2.7	18	72	14.2 ± 0.2	1.53 ± 0.02
	77°45.35′S			(11851)	(1055)	(5727)					(1.6 100)	0.21
Cathedral Rocks: Gothic profile												
R22640	162°39.48′E	1188	20	1.38	0.769	1.999	11	92.4 ± 5.2	12	18	13.1 ± 0.2	1.29 ± 0.02
	77°51.47′S			(10135)	(639)	(1660)					2.1 (103)	0.17
R22641	162°39.74′E	1079	21	1.38	0.642	1.868	9	82.4 ± 5.5	17	17	13.5 ± 0.2	1.31 ± 0.02
	77°51.31′S			(10135)	(477)	(1388)					1.8 (100)	0.17
R22642	162°40.52′E	977	20	1.38	0.727	2.302	33	76.7 ± 4.0	7	21	13.0 ± 0.2	1.32 ± 0.02
	77°51.21′S			(10135)	(573)	(1815)					2.0 (100)	0.19
R22643	162°40.77′E	843	21	1.38	1.194	3.772	<0.1	74.6 ± 4.8	21	34	12.9 ± 0.2	1.30 ± 0.02
	77°51.10′S			(10135)	(852)	(2691)					2.3 (100)	0.20
R22644	162°40.90′E	751	20	1.38	0.972	3.267	27	71.8 ± 3.4	5	29	12.7 ± 0.2	1.31 ± 0.02
	77°51.04′S			(10135)	(678)	(2279)					2.2 (102)	0.18
R22645	162°41.16′E	653	20	1.38	0.867	3.399	79	62.0 ± 3.3	<0.1	30	12.7 ± 0.2	1.39 ± 0.02
	77°50.99′S			(10135)	(472)	(1851)					2.2 (100)	0.18
R22646	162°41.29′E	477	21	1.38	0.570	2.709	29	50.3 ± 3.1	4	24	13.0 ± 0.2	1.31 ± 0.02
	77°50.94′S			(10135)	(351)	(1667)					2.1 (101)	0.20

AFT profiles that have experienced a relatively stable thermal and tectonic history (Gleadow and Duddy, 1981).

2.2. Apatite (U–Th)/He dating

(U–Th)/He dating is based upon the decay of U and Th via the production of α-particles (^{4}He nuclei) (e.g., Farley, 2002). Zeitler et al. (1987) showed that (U–Th)/He dating had considerable potential as a low-temperature thermochronometer after investigating He-loss in apatite and concluded that He-ages could be interpreted as cooling ages, with a closure temperature slightly lower than for fission tracks in apatite. Closure temperature varies with cooling rate (Dodson, 1973). The effective diffusion domain in apatites is the crystal size itself with larger crystals having a higher closure temperature (Farley, 2000; Reiners and Farley, 2001). Over geological time scales, He in apatite is retained at temperatures less than ~40 °C and is lost from the crystal lattice above ~80 °C (Wolf et al., 1996). This temperature zone (40–80 °C) corresponds to a shallow depth interval in the Earth's crust, known as the He partial retention zone (HePRZ) in apatite. The concept of an exhumed HePRZ can be applied to the interpretation of data in a similar fashion to that of an exhumed PAZ (Fig. 3). The closure temperature for the apatite (U–Th)/He system is usually quoted as 65–70 °C for typical rates of cooling and grain sizes (Farley, 2000). Other factors that must be considered when determining (U–Th)/He ages are: (1) the presence of U–Th rich inclusions within apatites that can result in anomalously old ages, and (2) α-particle emission from U and Th close to the edge of the crystal, as He is effectively lost and thus ages must be corrected depending on the crystal's size and shape (Farley et al., 1996).

All apatite (U–Th)/He ages were determined in the (U–Th)/He laboratory at Cal Tech. Apatite crystals were selected under an optical microscope at 110× following standard procedures (Farley, 2002) and on the basis of morphology, size (to determine F_T correction) and the lack of any visible inclusions or fractures. All results reported herein are on single crystals outgassed using a Nd–YAG laser. The absolute amount of ^{4}He was determined by isotope dilution using a measured volume of ^{3}He as a spike, in a quadrupole mass spectrometer. "Re-extracts" (Farley, 2002) (equivalent to a hot blank) were run following each analysis to test for the presence of (optically undetected) inclusions that were not completely outgassed. While most of the ejected He from these U- and Th-rich inclusions (e.g., zircon and monazite) is retained within the crystal, the inclusions themselves may survive the dissolution process thus contributing daughter ^{4}He to the analysis but not parent U and Th. If the "re-extract" had a ^{4}He signal above blank then the presence of a U- and/or Th-rich inclusion (that was not completely outgassed) was suspected and the analysis discontinued prior to the U and Th determination. It is, however, apparent from our data set that "re-extracts" do not always detect the presence of inclusions as a number of analyses (Table 2) gave anomalously old ages (tens to hundreds of million years too old). Outgassed crystals that passed the re-extract test were retrieved, dissolved in nitric acid and analyzed by ICP–MS to determine the absolute amount of U and Th using a double spike of ^{230}Th and ^{235}U (Wolf et al., 1996; House et al., 2001; Farley, 2002). The analytical uncertainty on (U–Th)/He ages was computed by adding in the uncertainty on the α-ejection correction and the uncertainty in the raw He age computed from the U, Th, and He measurement uncertainties, resulting in

Notes to Table 1:

Sample latitudes and longitudes are from the USGS 1:250,000 scale Ross Island and Taylor Glacier topographic maps. Parentheses indicate number of tracks counted (density) or measured (mean track lengths). Standard and induced track densities were measured on mica external detectors (geometry factor of 0.5), and fossil track densities were measured on internal mineral surfaces. Apatites were separated using conventional heavy liquid and magnetic techniques. Apatites were mounted in epoxy resin on glass slides, ground and polished to reveal an internal surface and then etched for 20 s at room temperature in 5 N HNO_3 to reveal spontaneous fission tracks. Ages were determined using the external detector method and an automated stage. Samples were irradiated in the X-7 position of the Australian Energy Commission HIFAR Research Reactor; Cd ratio for Au activation ~125. The mounts were counted at a magnification of ×1250, under a dry ×100 objective at the University of Melbourne. Ages were calculated using the zeta calibration method ($\zeta = 354 \pm 4.2$ for dosimeter glass SRM612), following the procedures of Hurford and Green (1983) and Green (1985). Errors were calculated using the "conventional method" (Green, 1981). The Chi-square test performed on single-grain data (Galbraith, 1981) determines the probability that the counted grains belong to a single age population (within Poissonian variation). If χ^2 is less than 5%, it is likely that the grains counted represent a mixed-age population with real age differences between single grains. The relative error or age dispersion (spread of the individual grain data) is given by the relative standard deviation of the central age. Where the dispersion is low (<15), the data are consistent with a single population, and the mean/pooled ages and the central age converge. Track lengths were measured using "confined" fossil fission tracks but only for those that were horizontal (Laslett et al., 1984) under a ×100 dry objective using a projection tube and a digitizing tablet attached to a microcomputer. Dpar (diameter of the track etch pit parallel to the *c*-axis) were measured under the same conditions. 5 Dpar measurements in 20 grains were collected for each sample; we report the mean and standard deviation of the 100 measurements.

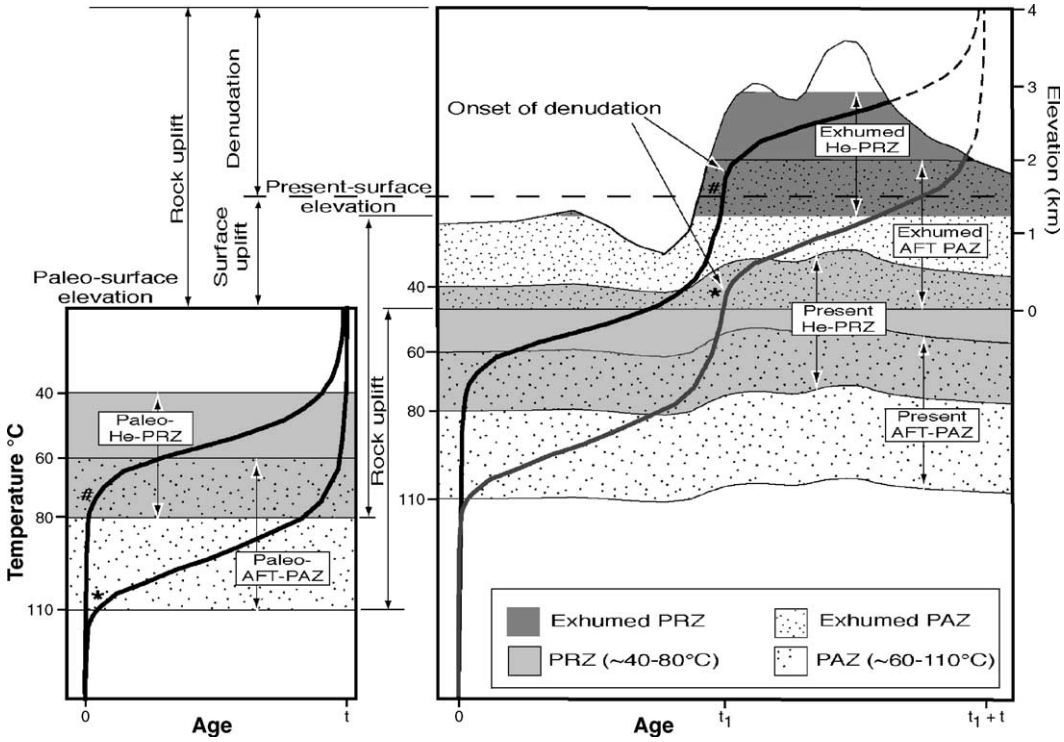

Fig. 3. The concept of an exhumed AFT-partial annealing zone (PAZ) and an exhumed (U–Th)/He-partial retention zone (PRZ) with respect to rock uplift, surface uplift and denudation. The shape and limits of the PAZ are after Fitzgerald et al. (1995) and the PRZ after Ehlers and Farley (2003). (a) In a relatively stable thermotectonic environment, the distinctive shape of a PAZ and a PRZ form over time t. In this example $t=100$ m.y. The distinctive shape of a PAZ is a result of the characteristics of track annealing (e.g., Green et al., 1986), whereas the distinctive shape of a PRZ is a result of an increase in the rate of diffusion of ^{4}He out of the crystal lattice with increasing temperature competing against the production of ^{4}He due to decay of U and Th (e.g., Farley, 2002). (b) At t_1, a period of cooling due to uplift and denudation occurs. If the cooling is relatively rapid compared to the previous period of relative stability, the break in slope in the age–elevation profile delineating the base of an exhumed PAZ (marked by an asterisk (*)) and the base of an exhumed PRZ (marked by the pound symbol (#)) indicate the onset of cooling accompanying rock uplift and denudation. This diagram is one dimensional, drawn to reflect only vertical motion with the AFT–age and He–PRZ profiles superimposed on idealized topography. The isotherms defining the top and base of the present day PAZ and PRZ reflect topographic effects and mimic a dampened topography (e.g., Brown, 1991; Ehlers and Farley, 2003). The AFT and (U–Th)/He ages defining the base of the exhumed PAZ and exhumed PRZ will be slight underestimates of the onset of rapid cooling, as samples defining the break in slope will have to cool through the PAZ and PRZ undergoing some annealing of tracks and some loss of ^{4}He. However, provided denudation (and hence relaxation of the isotherms) quickly follows rock uplift, this underestimation will be minimal. The (U–Th)/He profile is drawn for only one crystal size and for unzoned crystals (a range of crystal sizes results in a broadening of the width of the PRZ (e.g., Reiners and Farley, 2001) as does the presence of zoned crystals — see Fig. 10). The elevation of the base of an exhumed PAZ can be used to constrain the amount of denudation (Brown, 1991) and this same method is also applied to the base of an exhumed PRZ.

typical analytical errors of ±2.5% (1σ) (Ehlers and Farley, 2003). However, it is clear from theoretical studies and also examination of data presented herein that the dominant uncertainty in geologic samples is not the analytical error, but factors that cause variation in He-retentivity between different crystals (Ehlers and Farley, 2003), as discussed below in Section 3.

It is possible to use a more aggressive dissolution technique to deal with the effects of U- and Th-rich inclusions such as zircon and monazite. Such an approach would utilize standard procedures for the dissolution of silicate rocks (Potts, 1987). In this case, outgassed apatite grains and any inclusions are dissolved in HF, dried down and then put into solution with nitric acid for measurement of [U,Th] in the ICP–MS. In essence this yields a mixed apatite and inclusion (U–Th)/He age, dependent on the contribution of [U,Th] from each mineral phase. However, analytical techniques are not presently developed to distinguish the relative contribution from each phase.

2.3. Interpretation of AFT and (U–Th)/He data from vertical profiles

To interpret the cooling history using the AFT data we use the concept of "an exhumed PAZ" as revealed in

Table 2
(U–Th)/He single grain laser analytical data

	Elevation (m)	No. of grains	U (ppm)	Th (ppm)	He (nmol/g)	Radius (μm)	F_T	Uncorrected He age (Ma)	Corrected He age (Ma)	Error ± 2σ
Peak 1880										
R22615(a)	1054	1	19.654	35.273	5.700	57.1	0.767	37.424	48.806	2.73
R22615(c)		1	27.272	40.819	7.167	57.1	0.767	35.673	46.516	2.60
Mean			23.462	38.046	6.433		0.767	36.548	47.661	
Wt mean									47.61	1.14
R22616(b)	947	1	66.011	30.769	12.126	45.7	0.720	30.383	42.200	3.304
R22616(a)		1	86.580	40.032	19.432	45.7	0.719	37.128	51.638	4.073
R22616(d)		1	75.801	33.702	17.106	45.7	0.715	37.472	52.408	4.259
R22616(c)		1	58.646	34.607	14.107	40	0.678	38.740	57.110	6.030
Mean			71.759	34.777	15.693		0.708	35.931	50.839	
Wt mean									46.85	3.18
R22617(a)	847	1	26.888	38.349	5.561	57.1	0.757	28.438	37.572	2.255
R22617(c)		1	34.832	63.035	8.626	62.9	0.775	31.893	41.149	2.173
R22617(b)		1	21.493	44.985	5.825	51.4	0.727	33.339	45.859	3.416
R22617(d)		1	32.357	55.882	9.613	51.4	0.745	38.768	52.032	3.400
Mean			28.892	50.563	7.406		0.751	33.109	44.153	
Wt mean									42.25	2.83
R22618(a)	731	1	25.426	40.186	5.242	54.3	0.749	27.602	36.853	2.339
R22618(b)		1	28.766	55.846	6.204	45.7	0.715	27.196	38.026	3.085
Mean			27.096	48.016	5.723		0.732	27.399	37.439	
Wt mean									37.28	0.56
R22619(a)	636	1	53.708	51.258	10.186	54.3	0.759	28.437	37.467	2.215
R22619(b)		1	119.239	102.083	22.673	51.4	0.745	29.058	39.000	2.548
Mean			86.473	76.671	16.429		0.752	28.748	38.233	
Wt mean									38.13	0.76
R22620(d)	521	1	58.921	24.473	9.640	51.4	0.742	27.363	36.898	2.472
R22620(b)		1	65.221	35.423	10.216	40	0.687	25.504	37.132	3.688
R22620(c)		1	48.241	39.710	10.011	60	0.770	31.910	41.449	2.270
R22620(a)[a]		1	62.831	39.226	15.575	45.7	0.720	39.638	55.060	3.594
Mean			58.803	34.708	11.360		0.730	31.104	42.635	
Wt mean									38.99	1.58
R22621(a)	413	1	49.983	40.685	8.002	45.7	0.717	24.679	34.433	2.763
R22621(b)		1	34.117	20.163	6.410	60	0.772	30.276	39.213	2.114
Mean			42.050	30.424	7.206		0.744	27.477	36.823	
Wt mean									37.45	2.30
R22622(a)	299	1	65.576	67.292	12.611	57.1	0.763	28.448	37.297	2.148
R22622(b)		1	60.912	55.500	11.167	51.4	0.746	27.720	37.169	2.416
Mean			63.244	61.396	11.889		0.754	28.082	37.233	
Wt mean									37.24	0.06
Cathedral Rocks										
R22640(a)	1188	1	13.248	32.686	3.635	68.6	0.80	31.879	39.866	1.791
R22640(b)		1	19.445	60.945	6.316	51.4	0.74	34.328	46.476	3.181
R22640(c)		1	8.319	21.549	2.048	57.1	0.77	28.100	36.345	1.945
R22640(d)		1	20.790	47.893	7.240	57.1	0.77	41.442	53.784	2.932
R22640(e)		1	15.600	44.069	5.896	80	0.83	41.669	50.135	1.892
Mean			15.480	41.428	5.027		0.78	35.483	45.321	
Wt mean									43.80	3.17

(continued on next page)

Table 2 (*continued*)

	Elevation (m)	No. of grains	U (ppm)	Th (ppm)	He (nmol/g)	Radius (μm)	F_T	Uncorrected He age (Ma)	Corrected He age (Ma)	Error ± 2σ
R22641(a)	1079	1	13.466	77.959	7.056	63	0.765	40.730	53.240	3.016
R22641(b)		1	14.707	34.048	6.174	76.5	0.810	49.838	61.497	2.590
R22641(c)		1	24.590	51.952	7.778	76.5	0.808	38.777	48.019	2.057
R22641(d)		1	36.258	60.573	8.818	51.75	0.744	32.053	43.066	2.830
R22641(e)		1	22.888	49.230	7.246	63	0.765	38.577	50.454	2.866
Mean			22.382	54.752	7.414		0.778	39.995	51.255	
Wt mean									51.07	3.01
R22642(a)	977	1	20.998	49.273	8.581	58.5	0.764	48.289	63.204	3.605
R22642(b)[a]		1	25.781	69.501	33.399	54.3	0.741	144.362	194.874	13.133
R22642(c)[a]		1	31.143	64.975	32.322	99	0.848	126.867	149.532	5.237
R22642(d)		1	25.185	70.508	7.611	54.3	0.744	33.455	44.971	2.963
R22642(e)		1	30.277	62.661	7.544	47.3	0.720	30.773	42.757	3.355
Mean			25.487	60.814	7.912		0.740	37.506	50.311	
Wt mean									49.28	6.10
R22643(a)	843	1	22.466	46.203	6.030	72	0.814	33.212	40.798	1.683
R22643(b)		1	40.958	121.589	19.261	63	0.790	50.780	64.305	3.080
R22643(c)		1	72.894	263.668	32.734	65.3	0.777	44.521	57.307	2.990
R22643(d)		1	37.186	159.162	18.461	81	0.813	45.395	55.849	2.320
R22643(e)		1	29.937	41.066	7.297	76.5	0.823	33.824	41.096	1.614
Mean			40.688	126.338	16.757		0.803	41.546	51.871	
Wt mean									47.14	4.31
R22644(c)	751	1	8.844	25.561	3.907	135	0.890	44.725	54.171	1.571
R22644(d)[a]		1	6.027	14.740	12.240	99	0.851	233.034	273.934	9.512
R22644(e)		1	20.547	43.012	6.010	121.5	0.884	35.319	40.686	1.264
Mean			14.695	34.287	4.959		0.887	40.022	47.429	
Wt mean									45.99	6.59
R22645(a)	653	1	70.055	154.264	28.436	67.5	0.784	48.360	62.578	3.073
R22645(b)		1	27.702	48.041	6.254	54.3	0.755	29.057	39.019	2.345
R22645(c)		1	33.926	96.608	10.827	54.3	0.753	34.385	46.585	2.807
R22645(d)		1	21.962	60.264	7.874	49.5	0.735	35.260	54.430	3.334
R22645(e)		1	18.001	54.658	7.140	54.3	0.753	40.719	56.407	3.329
Mean			34.329	82.767	12.106		0.756	37.556	51.804	
Wt mean									49.80	4.38
R22646(a)	477	1	29.796	75.201	9.636	76.5	0.824	35.603	45.217	1.688
R22646(c)		1	25.864	50.499	6.348	72	0.816	29.699	37.829	1.479
R22646(d)		1	15.186	51.620	4.982	90	0.843	32.937	39.708	1.397
R22646(e)		1	27.944	71.823	9.944	81	0.832	39.104	48.938	1.767
Mean			24.697	62.286	7.728		0.829	34.336	42.923	
Wt mean									42.16	2.45

F_T is fraction of alphas retained (Farley et al., 1996); "corrected He ages" are corrected for this effect.

[a] These (U–Th)/He ages have been excluded from the determination of the mean or weighted mean. See text for explanation.

an age–elevation profile (Gleadow and Fitzgerald, 1987; Fitzgerald and Gleadow, 1990; Brown, 1991; Fitzgerald et al., 1995). We take into account any possible effects of advection of isotherms due to rapid denudation and also the deflection of near-surface isotherms due to topography (Stüwe et al., 1994; Mancktelow and Grasemann, 1997). The rates of denudation determined are low enough such that the effect on the geothermal gradient was minimal (e.g., Brown and Summerfield, 1997). However, topographic effects on near-surface geotherms (<100 °C) results in a relatively greater geotherm under valleys, compared to a depressed geotherm under ridges (Stüwe et al., 1994; Mancktelow and Grasemann, 1997; House et al., 1998, 2001; Stüwe and Hintermüller, 2000; Braun, 2002a,b; Ehlers and Farley, 2003; Reiners et al., 2003). Thus, denudation rates determined directly from a "vertical profile" down a valley wall or ridge may actually overestimate the true denudation rate because the age–elevation profiles are not strictly ver-

tical. The effects of topography on near-surface geotherms will be greater for the lower temperature thermochronologic systems and for those areas where the topographic wavelength is greatest (e.g., Stüwe et al., 1994). Note that we do not consider any spatial and temporal variations in the thermal field due to large magnitude normal faulting. Such variations have been documented along the Wasatch fault in Utah, where there was movement of ca. 10 km over ca. 12 m.y. (Ehlers et al., 2001, 2003). However, there is no single, large-magnitude range-bounding fault on the outboard side of the TAM, rather the Transantarctic Mountain Front is a zone of normal and/or dextral oblique slip faults (e.g., Fitzgerald, 1992; Wilson, 1999). The Cathedral Rocks and Peak 1880 profiles lie on the inland flank of the Discovery accommodation zone and while there are normal faults ~2 km from each of these profiles, offset on each fault is ~300 m, as indicated by an offset Ferrar Dolerite sill (Jurassic in age) and offset AFT ages. A transfer fault has been inferred to lie along the Ferrar Glacier (Fitzgerald, 1992; Wilson, 1999), but vertical offset along this fault is also considered relatively minor.

To correct the rates of denudation determined from age–elevation profiles, we follow the approach of Reiners et al. (2003) who used a 2D model of steady-state temperature distribution in the upper crust. However, in our case, we can ignore advection of isotherms due to denudation, as the low denudation rates we obtain from this part of the TAM will not significantly perturb the isotherms. We use Fig. 6 of Reiners et al. (2003) to calculate the admittance ratio (α; the ratio of relief on closure temperature isotherms to relief of the topography (Braun, 2002b)) for the AFT data and also for the apatite (U–Th)/He ages. The admittance ratio is largely dependent on topographic wavelength (λ) and only slightly dependent on topographic relief. For long topographic wavelengths, α is large and the correction of the denudation rate obtained from an age–elevation profile is greatest (Reiners et al., 2003). For a topographic wavelength of ~12 km (Fig. 2) the 65–70 °C isotherm (closure temperature isotherm for apatite in the (U–Th)/He system) is deflected about 25% of the topographic relief (i.e., α is ~0.25) and the ~100 °C isotherm deflected about 10% (i.e., α is ~0.1) (Reiners et al., 2003, Fig. 6). In order to correct the apparent denudation rate (measured age–elevation profile slope) for the effects of topography on isotherm depth, the factor $(1-\alpha)$ is multiplied by the apparent denudation rate. In our case, this correction factor will actually be an "over-correction" as our vertical profiles do not span the entire elevation range within the topographic wavelength and the vertical profiles were collected over the steepest part of the topographic wavelength. The steep U-shaped glacially sculpted walls of the Ferrar Glacier with slopes in excess of 30° (Fig. 2) are as close to "true" vertical profiles as is possible to collect in nature. In addition, correcting for topographic effects based on 2D cross-sections produces a maximum-correction because 3D topography does not defect isotherms as strongly as that depicted in 2D model calculations (Reiners et al., 2003). Another consideration is that we are correcting for the effects of paleo-topography based on existing topography, implying steady-state landforms since the Eocene. Nevertheless, this exercise is worth undertaking as it emphasizes the different parameters and the relative precision of using low-temperature thermochronologic data to constrain denudation rates and landscape evolution. The "maximum" correction factor for the AFT apparent denudation rate is therefore ~10% and for the apatite (U–Th)/He apparent denudation rate, ~25%. In our case a greater concern is the single grain (U–Th)/He age dispersion, and this is discussed below prior to any correction factor on the apparent denudation rate derived from the (U–Th)/He ages.

Another approach to constrain cooling histories for samples dated with multiple thermochronometers, is to divide the difference in closure temperature for each method (in this case ~30–35 °C) by the difference in ages; in this case AFT age minus the apatite (U–Th)/He age. We do not apply this method for two reasons. Firstly, this method "averages" the rate of cooling between the time each thermochronometer closes, and it is apparent from the age–elevation plots that there is a variable cooling/denudation history. Secondly, ages for samples resident in either a PRZ or PAZ for considerable lengths of time do not necessarily represent 'cooling' ages and thus assigning a closure temperature may be invalid. Thirdly, we have to deal with the age dispersion in the single grain (U–Th)/He ages before it is clear how to interpret (U–Th)/He ages for each sample. Another approach to constrain cooling/denudation histories is to create a pseudo-vertical profile for multi-thermochronologic systems. This method is discussed in Section 4.2, after we have evaluated intra-sample (U–Th)/He age variation. The variation in (U–Th)/He single grain ages also makes it difficult to use the elevation difference between identical AFT and (U–Th)/He ages to determine a paleo-geothermal gradient for that time. Note that errors on AFT and (U–Th)/He ages are quoted in the text as $\pm 1\sigma$, but drawn in figures as $\pm 2\sigma$.

2.4. Cathedral Rocks apatite fission track results and interpretation

AFT ages (Table 1) vary systematically with elevation, from 92 ± 5 Ma for the uppermost sample to 50 ± 3 Ma for the lowermost sample (Fig. 4a). Confined track length distributions (CTLD) have means of 12.7–13.5 μm and standard deviations of ~2 μm. Mean Dpar values for samples from this profile range from 1.27 to 1.35 μm with remarkably little variation between grains or between samples (Table 1), indicating little chemical variation between apatite crystals in these samples and between samples in this profile (Burtner et al., 1994; Donelick et al., 1999). The slope of the age–elevation curve (18 ± 2 m/m.y., ± 1σ) in conjunction with track length data suggest these samples resided within an apatite PAZ for long periods in the Late Cretaceous and Early Cenozoic prior to more rapid cooling. CTLDs tend towards bimodality, with the shorter tracks indicative of

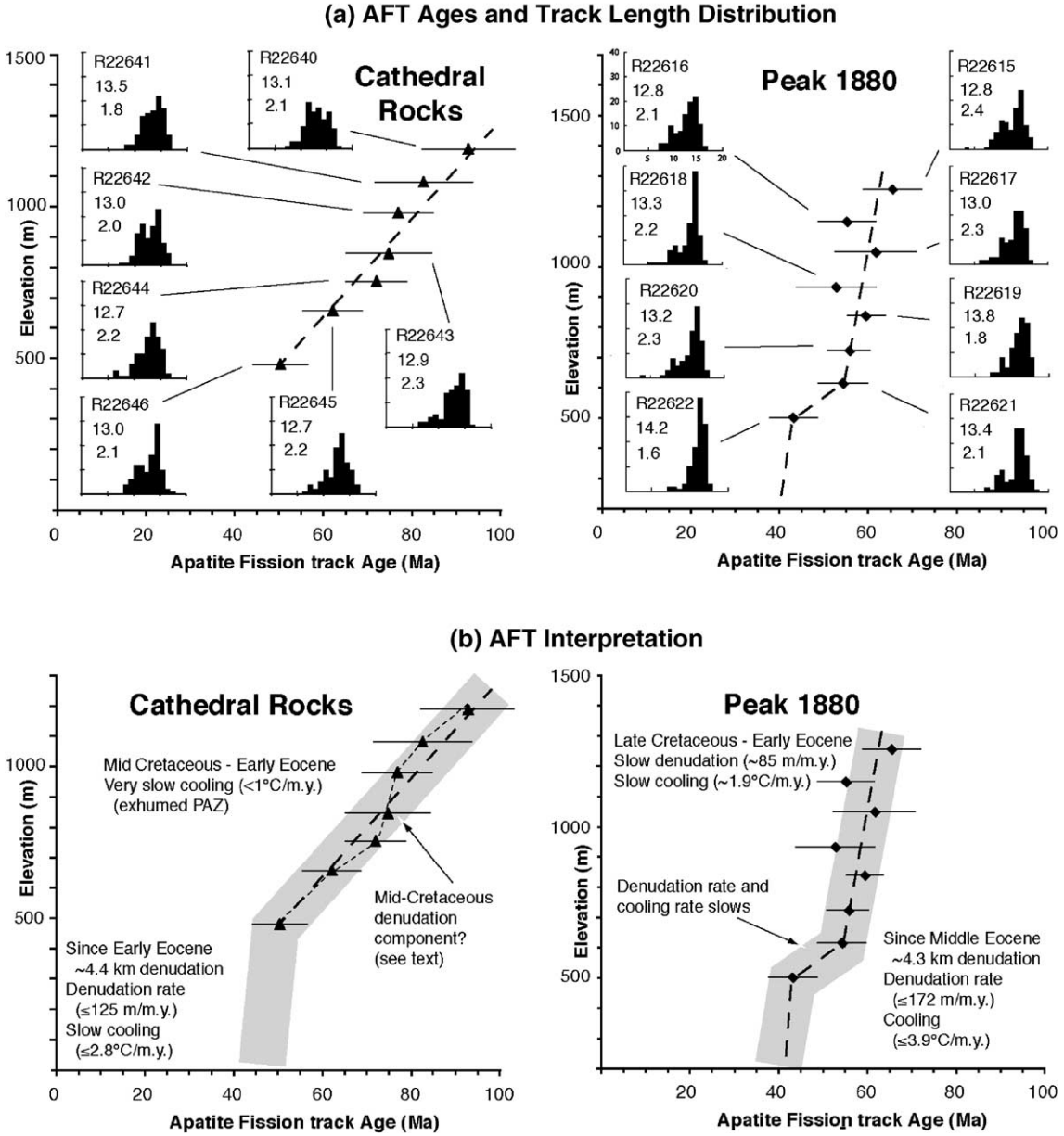

Fig. 4. (a) Apatite fission track ages versus elevation for vertical profiles from Peak 1880 and Cathedral Rocks. Error bars are 2σ. (b) Interpretation of the AFT data.

long-term residence in the PAZ in the Late Cretaceous to early Cenozoic and the longer tracks indicative of later "more rapid" cooling. It is not relevant to correct the slope of the curve (a corrected slope would be ~16 m/m.y.) for the effects of topography on the isotherms (as discussed above) as the slope largely represents a "fossil PAZ" (i.e., relative thermal "stability").

It is tempting to infer a period of mid-Cretaceous denudation from an inflection in the age–elevation curve (Fig. 4b), but given the uncertainties associated with the AFT ages, such a direct interpretation is beyond the resolution of the data. Results from detailed forward modeling of the Cathedral Rocks samples using Monte Trax (Gallagher, 1995) and AFTSolve (Ketcham et al., 2000) (AFT results shown in Fig. 5) show that the "good" and "acceptable" *T–t* paths indicate overall "slow cooling" in the mid-Cretaceous and Early Cenozoic (~50 °C in ~50 m.y. or a rate of ~1 °C/m.y.), prior to later more rapid cooling beginning in the early Eocene (~50 Ma). Closer examination of the modeled "good" and "best-fit" *T–t* paths suggest an apparent faster cooling in the mid-Cretaceous (~95 Ma to ~75 Ma) followed by residence of the samples for considerable periods of time within and near the base of a PAZ, prior to the later more rapid cooling beginning ~50 Ma. Note that there is a systematic difference in the form of the modeled cooling paths dependent on their relative crustal position and therefore the proportion of "Cretaceous to Early Cenozoic" (partially annealed) tracks compared to post-Early Cenozoic (i.e., longer tracks). In other words, samples low in the profile (R22646) provide little information on the mid-Cretaceous cooling as they have only a small proportion of those tracks, whereas samples high in the profile (R22641 and R22642) provide more information. While modeled *T–t* paths must be considered in totality, combined with the direct interpretation of the age–elevation profile, it is clear that the average rate of cooling through the Late Cretaceous to early Cenozoic is very slow, on the order of < 1 °C/m.y., but that there is likely a period of slightly faster cooling (denudation) in the mid-Cretaceous.

The amount of denudation since the early Eocene can be determined in a fashion similar to that done elsewhere along the TAM (Fitzgerald, 1992, 1994) using the base of the exhumed PAZ as the paleo ~110 °C isotherm (Brown, 1991). To constrain the amount of denudation, we use a paleo-geothermal gradient of 22.5 °C/km (Fitzgerald, 1992) for the "relatively stable" period just prior to when denudation began (~50 Ma). We use 22.5 °C/km for the paleo-geothermal gradient as this represents the mid-point of the range 20–25 °C/km previously constrained by Fitzgerald (1992) and simplifies the comparison between the two vertical profiles throughout the exercise below to determine the amount of denudation

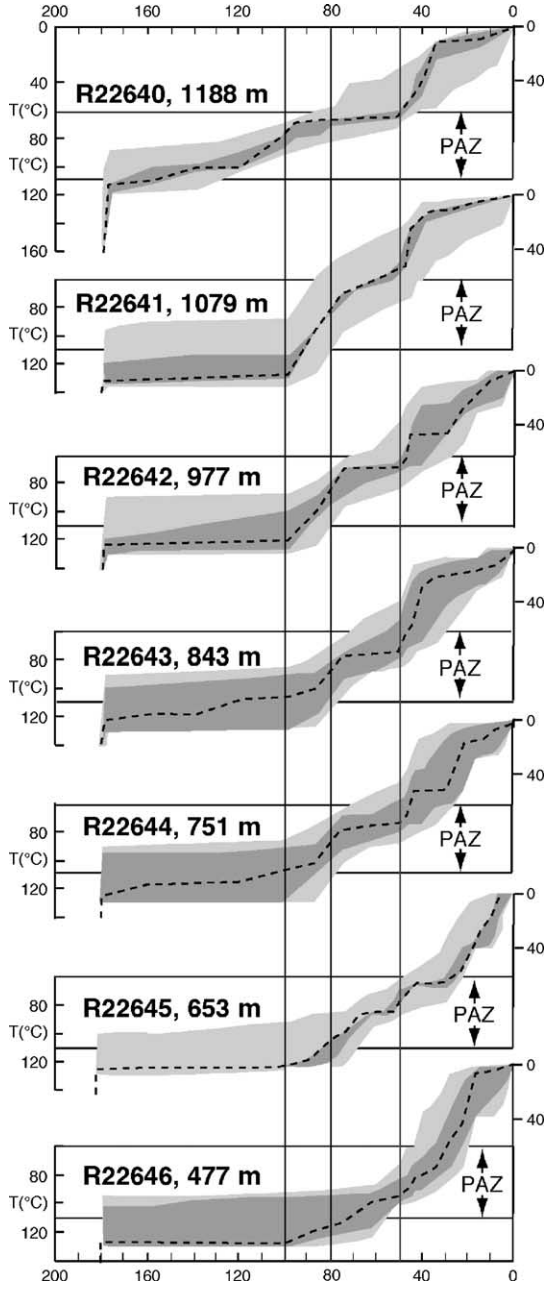

Fig. 5. Time–temperature models for AFT data from the Cathedral Rocks profile undertaken using AFTSolve (Ketcham et al., 2000). Samples are arranged according to their crustal position. Dashed line is the "best fit", dark gray envelope is a good fit (i.e., the *T–t* path is supported by the data) and light gray envelope is an "acceptable fit" (*T–t* path is not ruled out by the data). All models begin with rapid cooling following the Jurassic tholeiitic magmatic event that resulted in intrusion of thick dolerite sills and eruption of basalt at ~180 Ma (e.g., Elliot and Fleming, 2004).

(and hence average denudation rates) using the equation from Brown (1991). Calculated denudation amounts and rates therefore have at least a ±10% error. Conceivably, thermal modeling of samples in a vertical profile will produce modeled *T–t* paths from which a paleo-geothermal gradient can be constrained, but practically (Fig. 5) the best-fit envelopes do not allow a precise value to be determined. In addition, as we mention in Section 2.3, using the elevation difference between identical AFT and (U–Th)/He ages to constrain the paleo-geothermal gradient is complicated by the scatter of single grain (U–Th)/He ages. We discuss further the issue of paleo-geothermal gradients and how they influence our conclusions in Section 4.2. We use an elevation of ~0.4 km for the break in slope (determined from extrapolation of the best fit age–elevation line to when forward modeling indicates rapid cooling began), an early Eocene paleo-mean annual temperature of 0 °C, and a present day mean land surface elevation of 0.9 km. The amount of denudation since 50 Ma is therefore ~4.4 km, and the average denudation rate ~88 m/m.y. We do not apply a correction for the effects of topography to this average denudation rate, as it is not determined from the slope of the age–elevation profile. This average rate of denudation is slow enough so that advection will not perturb the isotherms (Stüwe et al., 1994; Mancktelow and Grasemann, 1997) and thus can be converted to an average cooling rate (using the same paleo-geothermal gradient of 22.5 °C/km) of ~2 °C/m.y. However, from geomorphic constraints and cosmogenic surface dating, the rate of erosion and landscape development in the Dry Valleys area are known to have been extremely slow (0.1–1 m/m.y.) since ~15 Ma (Marchant et al., 1993; Sugden et al., 1995a,b; Marchant et al., 1996; Summerfield et al., 1999). Assuming near-zero denudation since 15 Ma, the rate of denudation from 50 to 15 Ma can be constrained as ~125 m/m.y., which converts to an average cooling rate of 2.8 °C/m.y. Note however that the Ferrar Glacier is presently an active wet-based glacier and so the rate of erosion along the Ferrar Glacier is certainly greater than within the Dry Valleys, thus the average rate of cooling between ~50 and ~15 Ma would lie between 2 and 2.8 °C/m.y., or ≤2.8 °C/m.y.

To summarize, the AFT data from Cathedral Rocks indicates that since the early Eocene the rate of cooling was slow, likely ≤2.8 °C/m.y., but it changed from an even slower cooling regime prior to ~50 Ma when the cooling rate was <1 °C/m.y. Cooling rates determined using the AFT data bear directly on the interpretation of the age dispersion in the apatite (U–Th)/He single age grain data, as discussed below.

2.5. Peak 1880 apatite fission track results and interpretation

AFT ages from Peak 1880 (Table 1) also vary systematically with elevation, from 66 ± 3 Ma for the uppermost sample to 43 ± 3 Ma at the base of the profile (Fig. 4a). Mean Dpar values for samples from this profile range from 1.37 to 1.55 μm, slightly greater than at Cathedral Rocks, but again indicative of little chemical variation (Burtner et al., 1994) between crystals or between samples in this profile (Table 1). With the exception of the lower sample, all CTLDs tend towards bimodality and have means <13.8 μm and standard deviations >1.8 μm, indicating these samples cooled relatively slowly through the apatite PAZ prior to later more rapid cooling. A best-fit regression line through the upper seven samples gives a slope of 94 ± 47 m/m.y. (± 1σ). We can apply the $(1-\alpha)$ correction factor for the effects of topography on the geotherms, obtaining a mean denudation rate of ~85 m/m.y. for the upper part of the profile from ~66 to ~55 Ma. This rate is slow enough so that advection will not perturb the isotherms (Stüwe et al., 1994; Mancktelow and Grasemann, 1997), and thus we can constrain the rate of cooling of these samples as ~1.9 °C/m.y., using a paleo-geotherm of 22.5 °C/km. In contrast to the uppermost samples, the lowest and youngest sample (43 ± 3 Ma) has a CTLD (mean = 14.2 μm, S.D. = 1.6 μm) with a much-reduced component of shorter tracks. This indicates either that this sample resided close to the base of a PAZ prior to more rapid cooling, and/or relative to other samples in the profile spent comparatively less time cooling through the PAZ compared to the amount of time at cooler temperatures when track annealing is minimal. The shape of the age profile, the presence of short tracks in this lowermost sample, as well as the dominant long track component, combined with forward thermal modeling indicates that the rate of cooling probably slowed at ~55 Ma, but then increased at ~40 Ma (this is confirmed by the apatite (U–Th)/He data below). We can repeat the calculation performed on the Cathedral Rocks profile in order to constrain the cooling rate at Peak 1880 since ~40 Ma. Using the same paleo-geothermal gradient of 22.5 °C/km with the base of the break in slope at 0.2 km, the amount of denudation since 40 Ma is constrained as ~4.3 km. Thus, the average rate of denudation since ~40 Ma was 108 m/m.y. or between ~40 Ma and ~15 Ma, 172 m/m.y. (Fig. 4b). These denudation rates are slow enough so that advection will not perturb the isotherms and we can therefore constrain the cooling rate 40–15 Ma, assuming limited denudation after that time, as 3.9 °C/m.y. and as ≤3.9 °C/m.y. from ~40 Ma to recent. After

discussion of age variation in the (U–Th)/He ages later in the paper, it is apparent that the cooling rate implied by the (U–Th)/He ages below 800 m elevation is likely >7 °C and perhaps higher for the late Eocene (Section 4.2), greater than the AFT-determined average from mid-Eocene to mid-Miocene.

In summary, AFT data from Peak 1880 indicate slow cooling (~1.9 °C/m.y.) from ~66–55 Ma, possibly a slowing in cooling rate until ~40 Ma, followed by an increase in cooling rate (~4 °C/m.y.). In contrast, the AFT data from Cathedral Rocks indicate long-term residence in an apatite PAZ (a cooling rate of <1 °C/m.y.) from ~100 to ~50 Ma, before slow cooling (rate of ≤2.8 °C/m.y.) beginning ca. 50 Ma.

2.6. Cathedral Rocks apatite (U–Th)/He results

(U–Th)/He ages on single crystals from the Cathedral Rocks vertical profile range from 274 Ma to 36.4 ± 0.7 Ma (Table 2 and Fig. 6). Three single crystal ages of 150, 194 and 274 Ma are significantly older than all other grains, as well as their respective AFT ages and are therefore excluded from the data set due to the probable presence of previously undetected U- and Th-rich inclusions (see Sections 3.1 and 3.7). We note, however, that re-extracts on these analyses did not exceed hot-blank levels. Removing these three anomalously old grains still leaves a significant variation in single crystal ages for individual samples that is significantly greater than the analytical error. To gauge the variation of single grain ages we determine the standard deviation of the mean of single crystal ages for each sample expressed as a percentage of the mean. For the Cathedral Rocks profile, this ranges from 11% to 20% with an average of 16%.

2.7. Peak 1880 apatite (U–Th)/He results

(U–Th)/He ages on single crystals range from 34.4 ± 1.2 to 57.1 ± 2.6 Ma (Table 2 and Fig. 6).

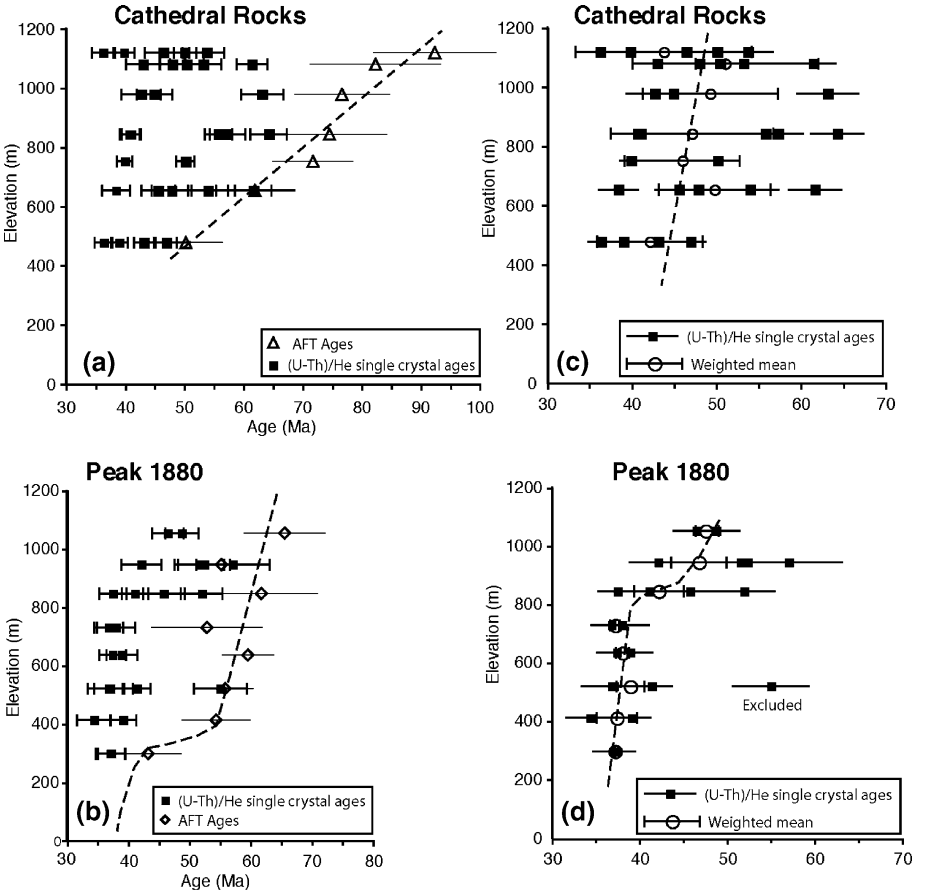

Fig. 6. (a and b) (U–Th)/He single crystal ages versus elevation for vertical profiles from Peak 1880 and Cathedral Rocks. AFT data is plotted for reference. Error bars are 2σ. (c and d) Single crystal apatite (U–Th)/He ages (error bars are 2σ, there are no ticks on the error bars) and the weighted mean for each sample (error bars are 2σ, there are ticks on the error bars) plotted versus elevation. Best-fit lines are plotted "by eye", although the slopes of the linear segments are determined by least squares regression.

The variation of single grain ages is less than that observed in samples from Cathedral Rocks. This is especially true in the case of samples below 800 m elevation where one standard deviation of the mean for the single crystal ages is <10%. In contrast, the two samples above 800m have a greater variation with standard deviations of the mean at >12%. This contrast is explained below in the context of cooling rates as determined from the AFT data. The slower the cooling rate, the greater the variation of single grain (U–Th)/He ages. One crystal from sample R22620a, with an age of 55 ± 2.1 Ma, is an outlier as it lies off the trend defined by the rest of the ages, and is excluded, as discussed below in Section 3.7.

3. Interpretation of intra-sample variation in single crystal (U–Th)/He ages

The variation in apatite single crystal (U–Th)/He ages in this study clearly exceeds the analytical error. In this section, we explore factors that may be responsible for the intra-sample variation in single crystal ages from Cathedral Rocks and Peak 1880. These factors are: the presence of inclusions or fluid inclusions (Lippolt et al., 1994), variation in crystal size (Reiners and Farley, 2001), any effects due to α-particle correction (Farley et al., 1996), that the grain boundary may not be a zero-concentration boundary (Belton et al., 2004a), factors that impede diffusion of He from a crystal (Spencer et al., 2004), and the contribution of radiogenic helium from ^{147}Sm (Belton et al., 2004b) (Table 3). The effect of cooling rate on the variation of single crystal ages must also be considered as it is apparent that the slower the cooling rate or longer a sample has resided in a HePRZ, the greater the variation in single crystal (U–Th)/He apatite ages (Meesters and Dunai, 2002b).

Small variations in helium diffusivity can lead to large differences in predicted age (House et al., 1999). However, it is not known whether activation energy and therefore closure temperature vary as a function of apatite composition. While Wolf et al. (1996) noted a variation in activation energy of 30–39 kcal/mol in the apatite samples they studied, it was unclear whether this variation was real or due to analytical error (Farley, 2000). Farley (2000) undertook diffusion experiments only on Durango apatite, determining an activation energy of 33 ± 0.5 kcal/mol and $\log(D_0) = 1.5 \pm 0.6$ cm^2/s. The experimental data to determine how diffusivity varies with apatite composition does not yet exist.

3.1. Sample quality and U- and Th-rich inclusions

An important concern in the practical application of (U–Th)/He dating and the reproducibility of data is the presence of U and Th rich inclusions (see Section 2.2). Undetected, the presence of U- and Th-rich inclusions will usually lead to old and anomalous ages (Lippolt et al., 1994; House et al., 1997; Farley, 2002), or in the case of multiple single crystal ages from a sample, the presence of obvious outliers may also indicate the presence of inclusions. Although each crystal was subjected to optical inspection, micro-inclusions may be impossible to see under a binocular microscope.

Lithology and sample quality also play a role in whether apatite crystals are suitable for (U–Th)/He dating. Subhedral, needle shaped, broken or rounded grains are not ideal candidates for (U–Th)/He analyses. Certain rock types such as alkali granites, fine grained granitoids, most volcanics, metamorphic rocks and sedimentary rocks often contain apatites too small or with too many inclusions to allow accurate dating (Ehlers and Farley, 2003). For example, apatites from orthogneiss at Mt Barnes (Fig. 1) in the Kurki Hills contained micro-inclusions of monazite, too small to be seen optically but able to be imaged with a SEM. (U–Th)/He ages from this lithology could not be reliably reproduced, despite repeated analyses.

3.2. Fluid inclusions

Fluid inclusions are a well-known source of magmatic or metamorphic fluids derived from mantle or crustal sources, and may have a significant radiogenic ^{4}He component (e.g., Ballentine et al., 2002; Ballentine and Burnard, 2002; Dunai and Porcelli, 2002, and references therein). With a [U,Th]-rich mineral such as apatite or zircon, a high density of inclusions or a high [He] within the fluid would likely be required to effect (U–Th)/He ages, except when the ages are quite young (Farley, 2002). ^{4}He hosted within a fluid inclusion will be parentless, or considered as “excess He”. As such, the resulting apatite (U–Th)/He age will be anomalously old. Several studies have ascribed anomalously old (U–Th)/He ages to the presence of excess ^{4}He from fluid inclusions (Lippolt et al., 1994; Stockli et al., 2000). No fluid inclusions were observed in apatites from the Ferrar Glacier region during the grain selection process involving optical inspection, and we do not consider this further as a reason for variation of single crystal ages.

Table 3
Factors than may contribute to variations in intra-sample apatite (U–Th)/He ages

Contributing factor	Effect	Result	How to monitor or avoid	References
U–Th rich inclusions	Contributes "parentless" ^{4}He	(U–Th)/He ages are older than what they would be if U and Th-rich inclusions were not present.	Careful grain selection, characterize grain population using SEM, running re-extracts.	(Farley, 2002; Lippolt et al., 1994)
Fluid inclusions	Contributes "parentless" or "excess" ^{4}He	(U–Th)/He ages may be older than what they would be if fluid inclusions were not present.	Careful grain selection, characterize grain population using SEM, running re-extracts.	(Farley, 2002; Lippolt et al., 1994; Stockli et al., 2000)
Grain size variation	Apatite grain is the diffusion domain	Larger grains have a higher closure temperature (older age). Large variation in single grain ages may indicate slow cooling.	Select same size grains for comparison within or between samples or use grain size variation for information on cooling rate.	(Farley, 2000; Reiners and Farley, 2001)
F_T correction (α-particle ejection)	Daughter α-particles from parent U and Th within 20 μm of grain boundary may be ejected from grain	Need to correct for α-particle ejection, homogeneous [U,Th] is usually assumed.	Careful grain selection (not too small, good crystal shape) and measurement of grain.	(Farley et al., 1996)
U and Th Zonation (effect on F_T correction)	If grain is zoned with respect to [U,Th]	As the F_T correction assumes homogeneous [U,Th], if grain is [U,Th] "core-rich" the age will be overcorrected. If grain is [U,Th] "rim-rich" the age will be under-corrected.	Examine grain population in fission track mount or SEM.	(Farley, 2002)
Fractured grains	Fractures provide rapid diffusion pathways (effectively reduces "grain size")	Grain size is less than measured and ages are therefore not "corrected enough" (i.e. corrected ages are too young).	Careful grain selection.	
Broken grains	Broken grains mean that the assumed α-particle distribution upon which the F_T correction is based is not correct.	Unless broken parts taken into account, the F_T correction will typically over-correct the age as more daughter α-particles are assumed lost than actually are; age too old.	Careful grain selection.	
Apatite grain boundary is not a zero concentration boundary	Daughter α-particles are either implanted into the grain from adjacent mineral phase or diffusion of ^{4}He is inhibited.	Less ^{4}He is ejected or diffuses from the grain than expected; or additional ^{4}He is implanted. F_T correction too great; age "too old".	Thin section analysis of rock type to determine if this may be a problem.	(Belton et al., 2004a; Spencer et al., 2004)
^{147}Sm	^{147}Sm decays via α-particle decay to ^{143}Nd.	A component of measured ^{4}He (typically 0.1–10% of total) could be from ^{147}Sm decay. Will result in overestimation of ages (ages too old).	Monitor [U,Th], measure ^{147}Sm.	(Belton et al., 2004b)
Zonation and rate of cooling.	Interplay of α-ejection and diffusion modifies He-concentration profile. Diffusion more important if sample is slowly cooled through PRZ.	Spread of single grain ages can occur if grains are variably zoned, and single grain age variation is enhanced if rate of cooling is slow.	Measure single grain ages. Use multiple thermochronometers to constrain cooling rate.	(Meesters and Dunai, 2002b)
Rock type (alkali granites, volcanics, metamorphic, sedimentary rocks)	Non-suitable apatites (too small and/or too many inclusions).	Small grains mean a less precise F_T correction, non-detectable inclusions give anomalously old ages.	Avoid some rock types, careful grain selection.	(Ehlers and Farley, 2003)
Rock type (granites and gneisses)	Phases such as Fe-oxides, titanite, epidote have high [U,Th]. Can implant α-particles into apatite.	(U–Th)/He ages may be too old (possibly > AFT ages).	Thin section analysis of rock type. Limit (U–Th)/He analyses to when ages will be <100 Ma?	(Spencer et al., 2004)

3.3. Grain size

Farley (2000) determined that the apatite grain itself is the diffusion domain and that diffusive loss is controlled by loss perpendicular to the *c*-axis. For grains cooling at the same rate (e.g., 10 °C/m.y.) a grain with a radius of 60 μm has a closure temperature of ~70 °C, whereas a grain with a radius of 80 μm has a closure temperature of ~73 °C. A large variation in single grain ages correlated with grain size may indicate very slow cooling (Reiners and Farley, 2001).

We attempted to eliminate any potential single grain age variation due to grain size by selecting grains of a consistent size. If scatter of single grain ages was due to the variation of grain size and hence variation in the diffusion domain size, then larger grains should yield older ages. For samples from Peak 1880, there is no correlation of grain size with age and all samples from <800 m elevation essentially have the same age. At Cathedral Rocks, a weak correlation of grain size with age may exist (Fig. 7). However, to determine if grain size played a dominant role in causing the observed variation in (U–Th)/He single grain ages at Cathedral Rocks, we forward modeled (using the program Helium_Age_Calculation.llb (Farley, 2000) available from http://www.gps.caltech.edu/~farley/farley.htm) sample (R22645) that yielded the greatest variation in single grain ages (24 m.y.) with a variation in the radius from 50 to 70 μm. The modeled *T–t* history was based on existing constraints from AFT data as well geological constraints, and was also selected to accentuate any potential grain size effects. We did not include any mid-Cretaceous cooling, but held the samples isothermal for 130 m.y. following mid-Jurassic (180 Ma), when these samples were completely reset due to the thermal effects of the Ferrar magmatism (Gleadow and Fitzgerald, 1987; Fitzgerald, 1992), and then cooled at a rate determined by the AFT data. The resulting maximum-modeled age difference between grains of the measured sizes was 12.6 m.y. In order to obtain an age variation of 24 m.y. between these grain sizes (50 and 70 μm), they would have been held isothermal for 275 m.y., a scenario that is highly unlikely, given the Jurassic magmatic event at 180 Ma. Thus, while the variation of single grain ages in a few samples may in part reflect grain size variation, it is not the dominant factor that resulted in the observed intra-sample variation of single grain ages.

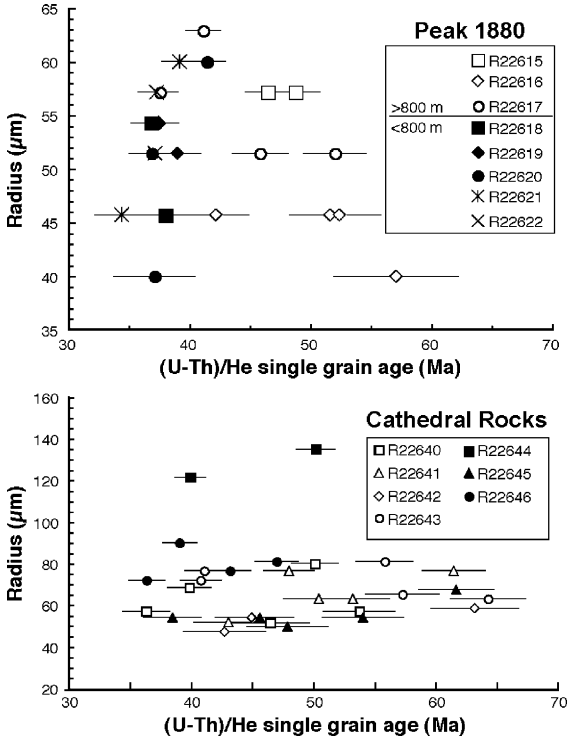

Fig. 7. Single grain ages versus grain radius for vertical profiles from Peak 1880 and Cathedral Rocks. For Peak 1880, note that for samples <800 m elevation, there is no variation of age with radius; we interpret these samples as relatively "rapidly" cooled. For samples >800 m elevation, single ages vary with radius; we interpret these samples as slowly cooled.

3.4. α-Particle emission (F_T correction), implantation and zonation

A well-known complication of (U–Th)/He dating is the spatial separation between the parent (U and Th) and the daughter product (α-particles) brought about by the decay mechanism. α-Particles in apatite are emitted by the U and Th series with sufficient kinetic energy (8 MeV) that they travel ~20 μm (Farley et al., 1996). Thus, some α-particles are ejected from the grain being analyzed. Farley et al. (1996) addressed this problem and developed a quantitative model for correcting He ages based on the size and geometry of the crystal. Two main assumptions are inherent in this correction factor (F_T parameter): (1) Implantation from the surrounding matrix is insignificant, so only α-ejection need be considered, and in most cases, the contrast between U–Th concentration in the mineral being dated and the matrix was considered so large that implantation was trivial (Farley, 2000). (2) The distribution of U and Th in the crystal should be specified, but as the distribution is generally not known, a uniform concentration of U and Th is universally assumed when making the correction. As the typical radius of apatite grains analyzed by (U–Th)/He dating is only a few

times greater than the stopping distance, a significant proportion, depending on the surface to volume ratio of the grain, of the α-particles is lost from the grain (Fig. 7). Correction of (U–Th)/He ages for α-particle ejection is based on grain size and assumes an idealized hexagonal geometry of the grain with a length/width ratio of three (Farley et al., 1996). Larger grains have a smaller uncertainty based on grain measurement and a smaller α-ejection correction factor or a greater proportion of α-particles (F_T) retained. Grains in this study have widths of 80 to 200 μm and thus the 2σ uncertainty on the α-ejection correction factor is ±9% to ±1% (Ehlers and Farley, 2003). This uncertainty is incorporated as part of the quoted analytical error for the (U–Th)/He ages.

If assumption (1) above is not strictly correct and the apatite grain lies adjacent to mineral phases with high [U,Th] that implants ^{4}He into the apatite grain (Spencer et al., 2004) a (U–Th)/He age that is too old will result because the implanted ^{4}He is "parentless" (i.e., parent U and Th lie outside the grain). If the apatite grain is in contact with a mineral phase that inhibits the ejection or diffusion of ^{4}He out of the grain (Belton et al., 2004a), the effect will be that less ^{4}He is ejected or diffuses from the grain than expected and the F_T correction will be an over-estimate and the resulting corrected age "too old". Spencer et al. (2004) examined (U–Th)/He ages (>100 Ma) from "slowly cooled" continental interiors and compared problematic samples (apatite (U–Th)He ages > AFT ages) to samples that appeared non-problematic (AFT ages > apatite (U–Th)/He ages). Problematic samples came from granitic and gneissic lithologies where apatite grains had contact with phases such as zircon, titanite and epidote with high [U,Th]. In contrast, non-problematic samples came from more mafic litholgies with phases such as feldspar, hornblende, biotites, and Fe-oxides that contained negligible [U,Th] adjacent to apatite grains. The implication from the Spencer et al. study is that the problematic samples are too old due to implantation of parentless ^{4}He into the apatite grains. In this study, it is possible that variation in single grain ages will be enhanced due to implantation of parentless ^{4}He in to the apatite grains, however we are unable to assess that effect.

As regards assumption (2), a uniform concentration of U and Th throughout the grain is typically assumed when correcting for α-particle loss. However, if the distribution of U and Th is non-uniform then the F_T correction will give an "erroneous age". If the grain has a higher [U,Th] core, especially if the majority of U and Th atoms are ≥1 stopping distance from the grain boundary, then the number of α-particles retained are greater than assumed and the F_T corrected age will be greater than the "true age" (i.e., over-corrected) (Farley et al., 1996; Farley, 2002; Meesters and Dunai, 2002b) (Fig. 8). If the grain has a high [U,Th] rim, especially if the majority of U and Th are ≤1 stopping distance from the grain boundary, then the number of α-particles retained are less than assumed and the F_T corrected age will be less than the "true age" (i.e., under-corrected). For example, a grain with radius of 60 μm retains 80% of its α-particles (F_T=0.8) and has a correction factor of 1.25 (1/0.8). However if the grain is zoned, with all the U and Th >1 stopping distance from the rim, then all the He is retained and the correction factor is 1 (i.e., no correction is needed). On the other hand, if all the U and Th are within 10 μm of the rim, the true F_T of this grain is ~0.65 and the correction factor 1.54. Thus, the proper correction factors to apply to these grains with differing zonation would be a minimum of 1 and a maximum of 1.54. However, assuming uniform U and Th distribution, we applied a correction factor of 1.25. Thus, if extreme zoning is present, it is possible to obtain a variation of ages approximately ±25% due to this effect alone. Thus, dating a number of grains that have different zonation patterns, but for which U and Th homogeneity is assumed, will result in a variation in single grain ages.

Distribution of [U] from a large population of grains from all Cathedral Rocks and Peak 1880 samples was determined qualitatively by examination of spontaneous and induced fission track density (^{238}U and ^{235}U, respectively). A correlation exists between spontaneous and induced fission track densities, as revealed in fission track mount-mica pairs (Fig. 9). However, it is not known whether Th and U, both parents for the ^{4}He daughter product, are spatially correlated within a grain in order to explain possible ^{4}He zonation. The distribution of U and Th within apatite grains would require investigation in order to determine if zonation of the parents, of which only U has been imaged by fission tracks, can be correlated and hence is responsible for zonation of ^{4}He. Notwithstanding this observation, it is apparent that zonation of U (and by inference Th) in samples from Peak 1880 and Cathedral Rocks is not ubiquitous; that is, zonation is relatively subtle and not extreme or concentric (i.e., exclusively rim-rich or core-rich U–Th zoned grains). We note that Hourigan et al. (2005) have developed a technique whereby they use an excimer laser to drill into a zircon grain to determine the zonation pattern of U and Th, and then assuming concentric zonation throughout the crystal, determine a modified F_T correction.

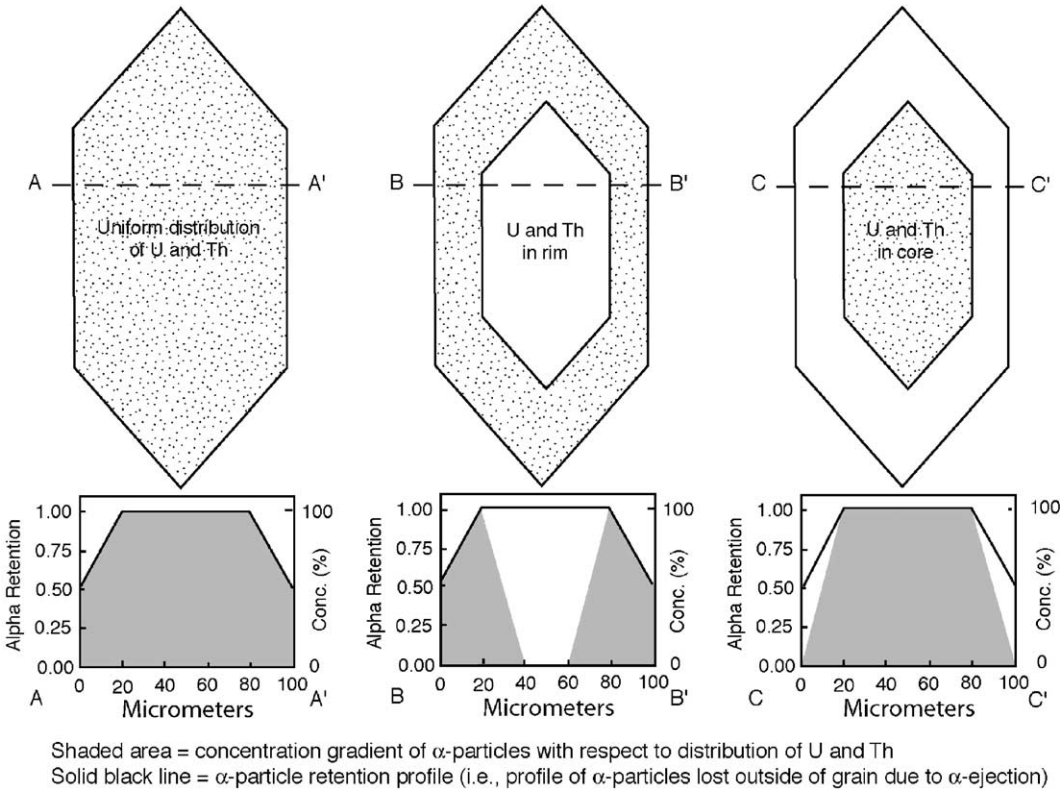

Fig. 8. He retention as a function of long stopping distance and variable distribution of U and Th for a rapidly cooled crystal in which α-particle ejection is important but loss of He due to diffusion is not. Schematic diagram is modified after Fig. 5 of Farley (2002). Stopping distance is taken as 20 μm (Wolf et al., 1996). U and Th distribution is shown in the upper part of the figure showing three scenarios: (a) uniform distribution, (b) all the U and Th in the outer part of the crystal<stopping distance of the rim, and (c) all the U and Th>one stopping distance from the rim. The lower part of the figure shows: (1) the α-particle retention profile (solid black line) that is independent of U and Th zonation, and (2) the resulting concentration profile (shaded area) for α-particle accumulation that is dependant on both U and Th zonation and the α-particle retention profile. From this figure, one can observe how different zonation patterns of U and Th may result in quite different ages purely due to the effect of α-particle emission. Assuming the same U and Th concentration in each crystal, (a) uniform distribution will give an intermediate age, (b) rim-rich will give the youngest age, and (c) core-rich will give the oldest age. The effects that diffusion (due to slow cooling through, or residence in the He–PRZ) has on the concentration gradient of α-particles for crystals with different zoning patterns and crystal geometries will magnify the age variation.

3.5. Samarium contribution

^{147}Sm is radioactive and decays via α-particle emission to the stable ^{143}Nd with a half-life of 1.06×10^{11} year (e.g., Faure, 1986). Once thought to be negligible, it has now been shown that modest amounts of Sm in apatite can contribute enough ^{4}He to make a significant contribution to the helium concentration (Belton et al., 2004b). ^{147}Sm-derived ^{4}He will typically contribute 0.1–10% total ^{4}He but in certain situations can exceed 25%. Thus, a systematic overestimation of (U–Th)/He ages may occur. Although it is obviously preferable to measure ^{147}Sm on the dated crystals, even without knowing [^{147}Sm], it is possible to estimate the ^{147}Sm-derived ^{4}He contribution from the total actinides (U and Th) concentration (Belton et al., 2004b). For apatites from Cathedral Rocks, the total actinides (U+Th) concentration ranges from 20 to 337 pm with an average of 94 ppm and a standard deviation of 61 ppm, thus the Sm-derived helium age contribution is on the order of 0.1–10% (Belton et al., 2004b). For apatites from Peak 1880, the total actinides (U+Th) concentration ranges from 54 to 221 pm with an average of 96 ppm and a standard deviation of 35 ppm, thus the Sm-derived helium age contribution is on the order of 1–8% (Belton et al., 2004b). However, the variation in single grain ages from these profiles is greater than the possible Sm-derived component. Samples above 800 m elevation from Peak 1880 have a range in ages up to a ±17–18% variation from the mean, or if expressed as a percentage of the minimum age, a range of 35–38%. At Cathedral Rocks

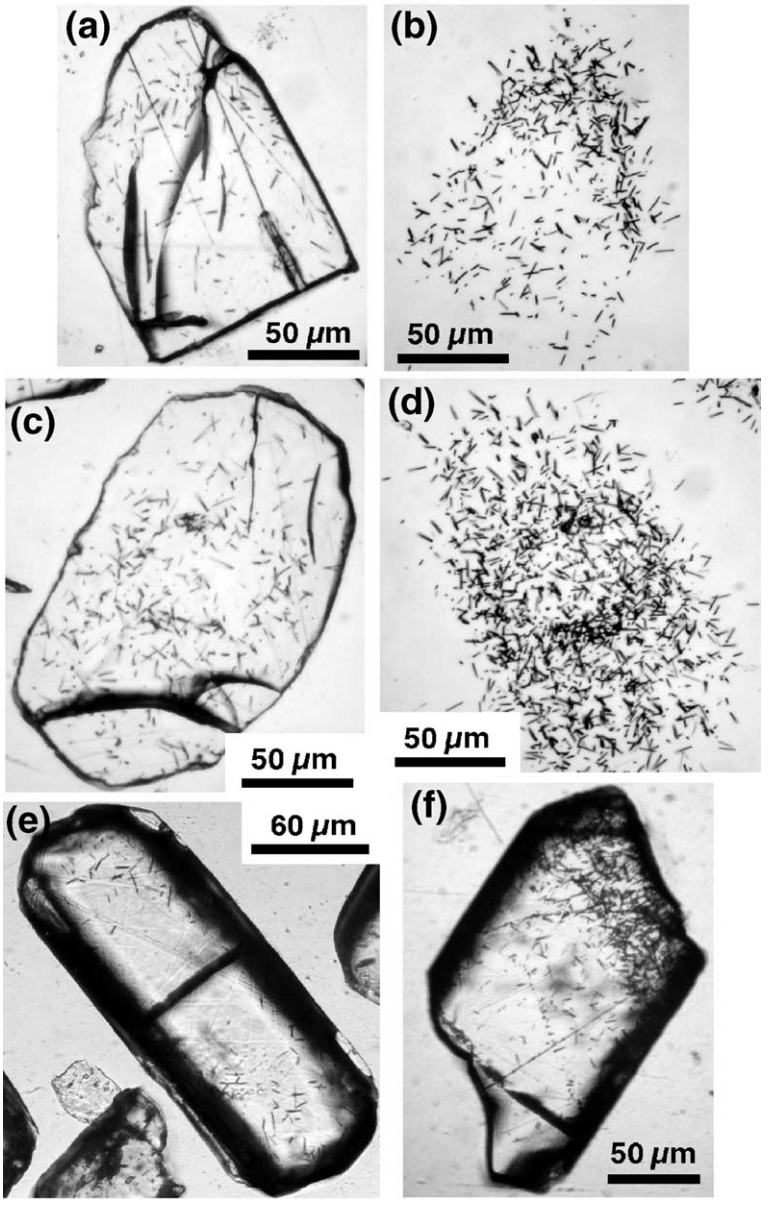

Fig. 9. Examples of zoned apatite grains. (a) A broken and zoned apatite crystal with etched fission tracks and its complementary mica-print replica in (b) showing etched induced fission tracks. Crystal is from sample R22616, from the Peak 1880 profile. (c) A core-rich zoned apatite crystal also from R22616 with etched fission tracks and the complementary mica-print replica in (d) showing etched induced fission tracks. Note that zonation is easier to see in the mica prints because of the higher track density and lack of other features such as cracks, polishing scratches, dislocations and defects. (e) A zoned crystal (a greater track density and hence U concentration at each end of the crystal) from sample R22645, from Cathedral Rocks. (f) Zoned crystal (note the greater track density at the top right end) also from sample R22645.

the variation in ages from the mean is typically greater than ±20%, or is expressed as a percentage of the minimum age, a range of 26–60%. Thus, the variation of single grain ages is too large to be solely caused by variable contribution of Sm-derived ^{4}He between grains; however, this may have caused a minor component of single grain age variation.

3.6. Cooling rate

As discussed above, the AFT thermochronologic results constrain the low-temperature cooling history of both vertical profiles. There is a general correlation between cooling rate and variation of single grain (U–Th)/He-ages. In general, when the rate of cooling

is >4 °C/m.y. the variation in single grain ages is much less than the variation of single grain ages when the rate of cooling is slower.

^{4}He escapes from the crystal lattice via volume diffusion (Wolf et al., 1996) and loss of ^{4}He by diffusion is augmented by loss of ^{4}He via α-particle emission. An apatite grain residing at temperatures higher than those at the base of a HePRZ will lose ^{4}He from the crystalline lattice as soon as it is produced whereas for an apatite grain residing at temperatures less than those at the top of the HePRZ diffusion of ^{4}He is very slow relative to its production. α-Particle ejection occurs at the grain boundary and thus the He-concentration gradient is not a step function but rounded (Farley, 2000). In a slow cooling scenario, a [U,Th] rim-rich grain will lose ^{4}He more readily (via α-ejection and diffusion) than a [U,Th] core-rich grain where loss is dominated by diffusion. When samples are slowly cooled or resident in a HePRZ for considerable periods, diffusion can potentially magnify the differences in He concentration profiles for rim-rich versus core-rich grains. Consequentially, the age variation between crystals of variable [U,Th] distribution becomes greater as the effects of diffusion become more important (Meesters and Dunai, 2002b).

Some forward models for production–diffusion of He in grains model diffusion first and then apply an α-correction factor (Warnock et al., 1997; House et al., 1999; Stockli et al., 2000). However, Meesters and Dunai (2002a,b) note that this method is likely to produce an over-correction of the modeled (U–Th)/He age if diffusion is important (i.e., samples have undergone slow cooling or have resided for considerable periods in the HePRZ). In contrast, the program DECOMP (a forward modeling program by Meesters and Dunai (2002a,b) used to calculate (U–Th)/He age evolution curves) models the effects of diffusion and α-particle ejection simultaneously. Meesters and Dunai (2002a,b) solve the production–diffusion equation for finite diffusion domains of various shapes and apply it to cases where distribution of U and Th is non-uniform and where diffusion is important (i.e., the case where samples spend a considerable amount of time within a HePRZ). A key finding of their study, relevant to our observations, is that when the distribution of U and Th (i.e., zonation) is varied from rim-rich to core-rich scenarios, they are able to produce a large variation in the modeled ages. We use DECOMP to model the variation of (U–Th)/He ages between rim-rich and core-rich grains in a HePRZ for apatite using the same "zonation patterns" used by Meesters and Dunai (2002a,b). Modeled isothermal *T–t* paths for samples with a variety of distributions of U and Th within the grain demonstrate the large variation in modeled ages in a HePRZ (Fig. 10). The greatest age variation in this somewhat artificial example (extreme zonation) is at the top of the HePRZ where ^{4}He loss is dominated by α-particle ejection at low temperatures with rim-rich grains yielding much younger ages than core-rich grains. Diffusion becomes the dominant loss mechanism at higher temperatures as shown by the shape of the He-age curve (rapid ^{4}He loss with increase in temperature) near the base of the HePRZ. When loss due to α-ejection dominates (i.e., a rim-rich grain), the subsequent loss via diffusion is comparatively less as both processes deplete the outer part more than the inner part (Meesters and Dunai, 2002b), hence the relatively greater ^{4}He loss at lower temperatures (relative to higher temperatures) for rim-rich grains. For a core-rich grain, diffusion will be the dominant loss mechanism, hence the comparatively greater ^{4}He loss ("reduction in age" in Fig. 10) at higher temperatures.

For (U–Th)/He analytical data, the correction factor for α-particle ejection (F_T correction — that assumes uniform U and Th distribution throughout the grain) is applied as a last step during the data reduction procedure. The F_T correction can enhance or magnify the variation in single grain ages. When grains of slightly varying U and Th distributions undergo slow cooling or prolonged residence in a HePRZ, the combined effect of α-particle ejection and diffusion will modify the He-concentration

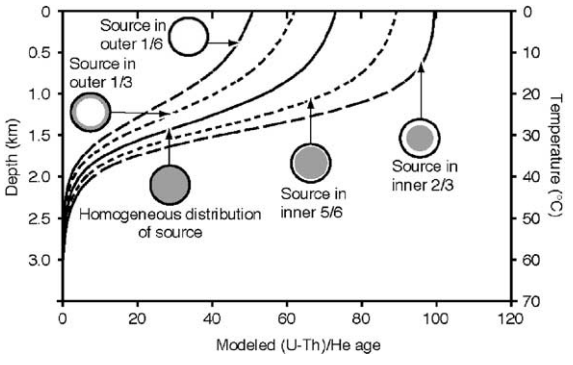

Fig. 10. (U–Th)/He age profiles for isothermal *T–t* paths (for temperatures from 0 °C to 62.5 °C modeled at 2.5 °C intervals over 100 m.y.) for different distributions of U and Th. The distributions modeled; uniform source throughout, source in the outer 1/6, outer 1/3, inner 2/3 and inner 5/6 are the same as those used by Meesters and Dunai (2002a,b). We used the program DECOMP by Meesters and Dunai (2002a,b) that models (U–Th)/He age evolution at 5 m.y. steps. This program uses a spherical geometry for the grain shape that approximates crystals of different shapes but with the same surface to volume ratio. We modeled a grain of radius 60 μm, which is about the same size as most of the crystals dated in this study. Activation energy used was E_a=33 kcal/mol with log(D_0)=1.5 cm^2/s (Farley, 2000).

gradient creating an even greater variation between rim-rich and rim-poor grains, as explained above. Thus, the F_T correction zonation-enhancement effect (see Section 3.5) is magnified by the residence within, or slow cooling through, a HePRZ, because the F_T correction assumes that all grains have a uniform U and Th distribution. Such a pattern is revealed in data from Peak 1880 and Cathedral Rocks. The "most rapidly" cooled samples in this study from below 800 m elevation on Peak 1880 show the least age variation (Fig. 6). Samples from Cathedral Rocks, where the cooling rate is slowest, show the most variation in single grain (U–Th)/He ages. The variation in single grain ages increases about 20% following the F_T correction for the Cathedral Rocks samples, whereas there is little apparent F_T correction age variation enhancement in those "more rapidly" cooled samples from Peak 1880 (Table 2).

3.7. Identification of outliers and exclusion of single crystal ages

In evaluating this (U–Th)/He data set we do not exclude data points unless it can be justified. Given their respective closure temperatures, a (U–Th)/He age is expected to be younger than or equal to its corresponding AFT age and as such this criteria can be used to screen for outliers. The criteria that we use to exclude (U–Th)/He data is appropriate if [U,Th]-rich inclusions, fluid inclusions or other factors (Table 3) can be shown to be the cause of anomalously old ages. There are, however, instances where apatite (U–Th)/He ages have been found to be older than AFT ages. Two scenarios for such a case have been identified:

(1) In the White Mountains of eastern California, Stockli et al. (2000) reported a situation where an AFT age from a sample ~5 m under an andesite flow was completely reset whereas the corresponding (U–Th)/He age was only partially reset and the He-age was significantly older than the AFT age, most likely because of the effects of short-term heating on the two systems. Stockli et al. (2000) concluded that AFT ages will be younger than He ages when the duration of heating is short compared to radiogenic ingrowth. Mitchell and Reiners (2003) found a similar effect where an "inversion" of AFT ages and apatite (U–Th)/He ages on the same samples occurred due to short-term annealing effects of wildfires. In our case, we think that neither volcanism nor wildfires are important. While there are Plio-Pleistocene cinder cones along the Ferrar Glacier, especially close to the coast (Wilch et al., 1993), the thermal effects of volcanism did not apparently reset, or partially the AFT ages. This is because, in our situation, we are discussing anomalously old single-grain He-ages that are outliers with respect to the rest of the single crystal ages from the same samples, rather than the He-ages from one sample all being partially reset. Likewise, neither the climate of Antarctica nor the vegetation (Francis, 1999), would have been conducive to wildfires resetting, or partially resetting these samples once they were exposed on the surface, especially when one considers that these samples were collected from steep glacially carved walls of the Ferrar Glacier.

(2) Reproducible but unexplained "anomalously old" apatite (U–Th)/He ages (i.e., older than the respective AFT ages) have also been reported in samples that are considerably older than 100 Ma (Crowhurst et al., 2004). While these authors have no definitive explanation for these old ages, they note that problematic samples may be related to depletion in LREE. Spencer et al. (2004) noted a relationship between problematic old (U–Th)/He ages and surrounding high [U,Th] mineral phases (Section 3.4). In contrast, Hendriks and Redfield (2005) have suggested that some AFT ages (ca. 300–700 Ma) in the Fennoscandian craton are younger than their corresponding apatite (U–Th)/He ages (ca. 400–600 Ma) due to radiation-enhanced annealing (or radiation-enhanced lattice repair) of fission tracks in apatites rich in α-emitter actinites. This does not appear to be relevant in southern Victoria Land apatites because the ages are geologically much younger than the Fennoscandian craton samples and the apatite (U–Th)/He single crystal ages exhibit a variation or scatter of ages, many of which are younger than the corresponding AFT age. We also found no systematic variation of [U,Th] concentration with apatite (U–Th)/He age.

It is intuitively easy to identify single crystal ages that are tens or hundreds of million years older than other single crystal ages in a sample as not belonging to the same population and therefore able to be discounted. Two samples from Cathedral Rocks (R22642 and R22644) have one or more crystal with a (U–Th)/He-age that are obvious outliers as the ages are ≥100 m.y. older than the other single grain ages (Table 2). These anomalously old single grain ages are rejected

on the basis that they must contain previously optically undetected U–Th rich inclusions that were not detected in the re-extract test (e.g., House et al., 1999; Stockli et al., 2000). To test whether single crystal ages belong to the same population, the criterion of Chauvenet provides an objective method to exclude suspected outliers (Long and Rippeteau, 1974). This criterion allows rejection if the probability of occurrence of data is less than $1/2n$ (n = number of values averaged). The data point is excluded, and a new weighted mean calculated. This approach is similar to that used in the removal of single crystal $^{40}Ar/^{39}Ar$ outlier ages resulting from incorporation of xenocrystic (older) and younger altered grains when dating volcanic rocks or ashes where any grain outside 2σ of the mean of the population is excluded, and a new mean calculated (e.g., Deino and Potts, 1990; Spell et al., 1996). The probability that grain R22620a from Peak 1880 (Table 2 and Fig. 6) belongs to the same population as other grains fails this criterion and is therefore excluded. It is probable that grain R22620a contained small or micro-inclusions, resulting in an age relatively close to the other ages in this population, but still outside the limit.

4. Discussion and practical considerations

The considerable variation in our single grain (U–Th)/He ages exceeds analytical error and can be correlated to cooling rate and residence time of the sample in the HePRZ. Neither the presence of inclusions nor grain size variation can reasonably explain the observed scatter of ages. We suggest that the variation of (U–Th)/He single grain ages obtained from the Peak 1880 and Cathedral Rocks vertical profiles, potentially due to a large number of variables (Table 3), is dominantly a function of U and Th zonation within apatites that creates different He-concentration profiles following decay via α-particle emission and loss of ^{4}He via diffusion. The He-concentration profile can also be altered by either external α-particle implanation or inhibition of ^{4}He diffusion from the grain. The apparent variation in single grain ages is enhanced when the α-particle ejection correction factor (F_T correction) is applied as this correction factor assumes uniform U and Th distribution throughout a grain.

We see a similarity between the intra-sample (U–Th)/He age variation in which age dispersion is related to cooling rate or residence time in a HePRZ and the well-known effects that variation in apatite chemistry has on annealing rate (and age dispersion) of fission tracks. In AFT thermochronology, one of the variables that controls the rate at which fission tracks anneal is the chemical composition of the grains (Gleadow and Duddy, 1981; Green et al., 1986; Donelick, 1991; O'Sullivan and Parrish, 1995). For example, fission tracks in Cl-rich grains are more resistant to annealing than fission tracks in fluorapatite. Thus, if there is a range in chemical compositions between grains, there will be a range of single grain ages with the variation of ages correlated to the cooling rate. If the grains cooled quickly, the variation of ages will be minimal. If the sample cooled slowly or resided in a PAZ prior to later rapid cooling, the variation of single grain ages is magnified. This is a common occurrence for AFT thermochronology applied to sedimentary rocks where apatite grains may have different AFT provenance ages as well as slightly different chemical compositions before long-term residence in a PAZ magnifies the variation in single grain ages. Chemical variation between grains that lead to significant age dispersion has also been noted in plutonic rocks (O'Sullivan and Parrish, 1995), however this is not the case for samples from these two profiles from southern Victoria Land as shown by the uniformity in Dpar values (Table 1).

If apatite grains are zoned with respect to U and Th and provided the resulting He-concentration profile is a result of this (i.e., ignoring variation of the He-concentration profile due to external factors such as implantation or diffusion impedance), and a representative number of grains are dated, the effects should be observable, systematic and predictable. The variation in single grain ages should be minimal if cooling is rapid, but as the cooling rate decreases the variation of single grain ages should increase. The variation of single grain ages should be less towards the base of the exhumed HePRZ, as loss via diffusion is the more dominant loss mechanism than loss via α-particle ejection. Towards the middle of an exhumed HePRZ, the variation in single grain ages should reach a maximum as relative loss via diffusion diminishes and relative loss via α-particle ejection increases. If samples resident within a HePRZ are all perfectly uniform in their distribution of U and Th there should be minimal variation in single grain ages, as each grain (ignoring grain size effect) will have the same He concentration profile.

Thus, in slowly cooled terranes, an intra-sample variation in single grain (U–Th)/He ages should not be completely unexpected. Use of multiple thermochronologic techniques to document the thermal history is obviously desirable, and if possible should be coupled with the use of vertical sampling profiles collected with respect to relevant structures to better constrain the thermal and tectonic history. AFT thermochronology

and apatite (U–Th)/He dating comprise a natural complementary pair of techniques as they are the two lowest temperature techniques commonly used, they use the same mineral, and modeling programs based on laboratory annealing or diffusion annealing experiments are available (Gallagher, 1995; Carlson et al., 1999; Donelick et al., 1999; Ketcham et al., 1999; Farley, 2000; Meesters and Dunai, 2002b).

As with other low-temperature thermochronologic techniques, it is often assumed that (U–Th)/He ages simply reflect the time that a sample cooled through a certain closure temperature. However, all too often such an interpretation, while attractive in its simplicity (e.g., when using AFT–(U–Th)/He pairs to determine cooling rates) is incorrect. Samples may reside in the crust within PRZs for extended periods of time. As such, an (U–Th)/He age by itself may be geologically meaningless (cf., Lister and Baldwin, 1996). It is the interpretation of a suite of data utilizing multiple thermochronologic techniques, especially if samples are collected in a vertical profile, which allows one to determine the most likely *T–t* path. The most useful thermochronologic techniques for tectonic studies have a kinetic parameter in addition to an age that allows the *T–t* path to be constrained. Examples of these are confined track lengths in AFT thermochronology (Gleadow et al., 1986) and age spectra, arrhenius and log r/r_0 plots for $^{40}Ar/^{39}Ar$ thermochronology (Lovera et al., 1989). A (U–Th)/He age is a total fusion age (cf., K/Ar ages), although the intra-sample variation of single grain ages and variation of age with respect to grain size (Reiners and Farley, 2001) can potentially be used to constrain the cooling history of a rock. A variation on the (U–Th)/He technique involves proton-induced ^3He that allows $^4He/^3He$ dating using a step-heat approach and should provide information on the *T–t* history of the sample (Shuster and Farley, 2003; Shuster et al., 2003). This $^4He/^3He$ step-heat method may also be useful in resolving "excess-He" problems. For example, excess Ar from fluid inclusions in K–Ar dating and $^{40}Ar/^{39}Ar$ thermochronology is a well-known phenomena often observed in the lower temperature steps of Ar–Ar step heat experiments (e.g., Kelley, 2002 and references therein), and "excess He" may be revealed in lower steps of $^4He/^3He$ spectra. Likewise, "excess He" from solid-state inclusions (zircons, monazite) may be revealed in the higher temperature steps.

Owing to the unique nature of the (U–Th)/He technique in which grains are outgassed for He and then dissolved to measure U and Th, it may be impractical and unnecessary to image or scan all apatite grains for U and Th zonation before an (U–Th)/He age is determined. Spontaneous and induced fission track distributions along with SEM or electron microprobe analysis to determine [U,Th] will only give a 2D image of the zonation pattern if present. U and Th zonation need not be concentric (see Fig. 9). If grains are imaged prior to (U–Th)/He dating, the F_T correction factor will have to be modified to reflect the removal of one grain face — introducing another source of error.

4.1. Weighted mean versus minimum age of single grain ages?

In other thermochronologic or geochronologic techniques such as single crystal $^{40}Ar/^{39}Ar$ dating of volcanic ashes (e.g., Deino and Potts, 1990; Spell et al., 1996) a mean or weighted mean of the single crystal ages is often used. Most AFT ages are determined using the external detector method and central ages (the population geometric mean age) calculated (Galbraith and Laslett, 1993). A Chi-square test is then applied to determine if single grain ages (~25 per sample are routinely calculated) fall within a Poisson distribution and thus belong to a single age population (Galbraith, 1981). The Chi-square test, plus age dispersion (relative standard deviation of the population ages), describes the distribution of population ages. However, non-Poissonian variation is often present in AFT determinations as a result of grains from multiple sources (e.g., sedimentary rocks) and differential annealing between grains of slightly differing chemical composition that lead to mixed ages, but these are taken into account using the central age.

No such "weighted mean" approach has yet been applied to (U–Th)/He ages, probably because such a variation in single grain ages has not been previously documented in the literature. In fact, where the cooling history is simple, apatite (U–Th)/He ages are very reproducible within analytical error (Ehlers and Farley, 2003). How representative is a weighted mean age compared to the most representative or "true" (U–Th)/He age? Have we captured the full distribution of single grain ages from Peak 1880 and Cathedral Rocks (Fig. 6); that is, are our measured ages a representative subset of the true single grain population? If enough single grains were dated, would we ideally obtain a continuum of ages with a Poisson distribution centered on the weighted mean? In the case of (U–Th)/He dating, however, it is clear that complicating factors (Table 3) such as the presence of U- and Th-rich micro-inclusions, compositional zonation, ^{147}Sm decay-contributed ^4He and either external α-particle implantation or inhibition of ^4He diffusion can result in older (U–Th)/He single crystal ages. This implies that where there is a variation

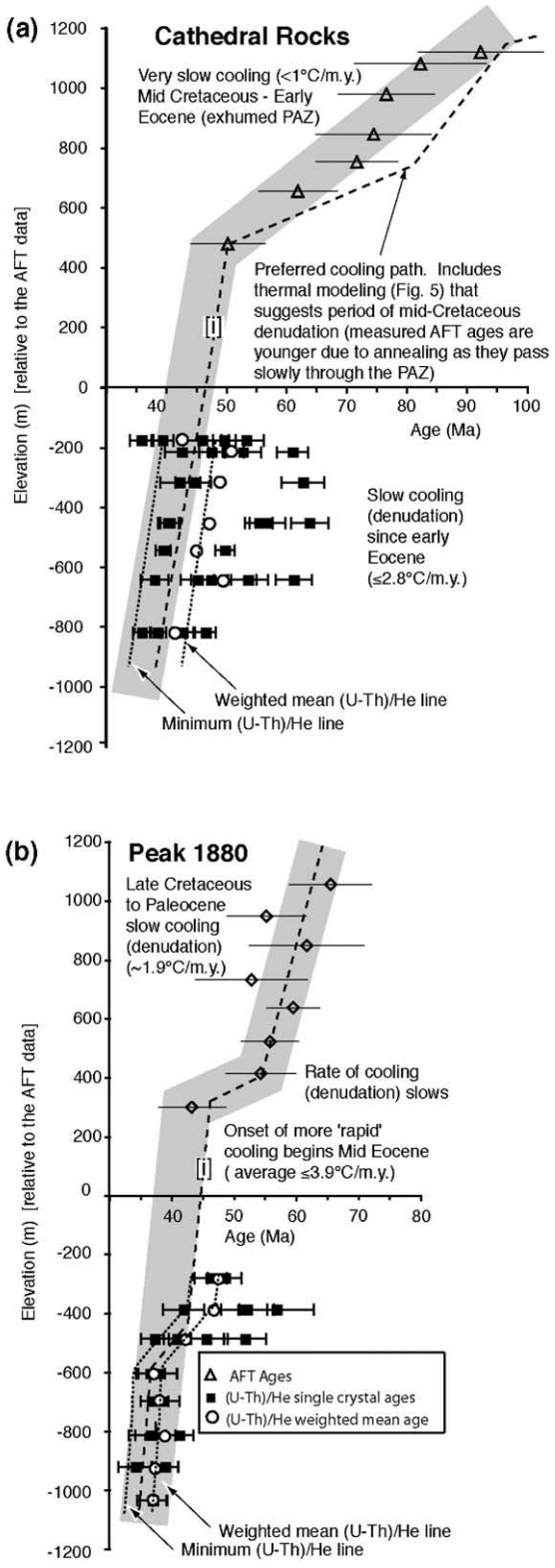

of single grain ages, it is the younger ages in the population that are actually closer to the "true" age and that the older ages may result from a combination of various complicating factors. However, the weighted mean (U–Th)/He age for some samples are older than the AFT central ages and older than the AFT model-derived cooling path (Fig. 11). We do not regard the AFT ages as being "too young" due to thermal- or radiation-induced annealing. In addition, the youngest (U–Th)/He age (or minimum line) cannot be regarded as the "true" age because of the possibility that the youngest ages are represented by rim-rich grains, that in a slow cooling scenario yield ages that are too young. Experience has shown that grain populations are not systematically zoned, grains are not all core-rich, nor rim-rich, nor have concentric zonation patterns, but are more likely to be a combination of unzoned and variably zoned crystals. Thus, the "true" age likely lies between the weighted mean (U–Th)/He age and the youngest age (or minimum age line). Therefore, we suggest that once outliers due to the presence of U- and Th-rich inclusions are excluded (Section 3.2), a weighted mean age is determined and that the weighted-mean best-fit line is used to guide the placement of the minimum (U–Th)/He line, and that the "true" age trend will lie between these two. In a simple relatively rapidly cooled situation, the youngest age and the weighted mean age will likely lie within error, and as cooling rate decreases, the two will diverge (Fig. 11). Only in a slowly cooled situation, such as in these samples from the TAM is single crystal age variation likely to be a problem.

How then to determine which is the "true" or most representative (U–Th)/He age for samples from the Cathedral Rocks and Peak 1880 profiles that display significant single crystal age variation? A "true" age may be impossible to delineate unless we are sure we have captured the full variability in the single crystal ages. For most samples, we have obtained 4–5 grains, but for some samples, there are only two single grain ages. In the Syracuse (U–Th)/He lab, the standard procedure is to determine five single crystal ages, and in most geologic situations this number of single crystal

Fig. 11. Composite AFT and apatite (U–Th)/He plots summarizing cooling information and preferred denudation curve for (a) Cathedral Rocks and (b) Peak 1880. Thick grey line marks the generalized denudation curve as determined from the AFT data. Dotted lines mark the weighted mean (U–Th)/He best-fit line and minimum (U–Th)/He line. Note that where the rate of cooling is more rapid (Peak 1880 compared to Cathedral Rocks) these two lines become closer. Dashed line [i] is the preferred cooling path for each profile as discussed in the text.

ages will probably be sufficient. Yet, where samples are slowly cooled and the rate of denudation is very slow, such as in these samples from the TAM, the full age variability is only likely to be robustly constrained if 20–25 single crystal ages are determined, this number selected only by analogy with AFT thermochronology. The precision of (U–Th)/He ages and the measure of true single crystal age variability will also be better constrained if other variables such as measurement of ^{147}Sm during ICP–MS analyses (as is now routinely done in some labs) and a characterization of [U,Th] zonation in the crystal population or the actual crystal analyzed is undertaken.

4.2. Multi-chronometer composite vertical profiles

Provided the regional geothermal gradient has remained relatively stable throughout the time period covered by the different thermochronologic data it is possible to construct a composite vertical profile combining data from apatite (U–Th)/He ages and AFT thermochronology. In this study, the calculated average cooling rates determined from the AFT thermochronology are slow enough that advection of isotherms is of minimal concern. A composite profile permits better constraints on the denudation history, allows us the opportunity to evaluate the interpretation of the single grain (U–Th)/He ages and serves as a summary figure (Fig. 11). Composite profiles are constructed by changing the relative elevations of one of the methods (in this case apatite (U–Th)/He ages) by the difference in closure temperatures (30–35 °C) divided by the paleogeothermal gradient (22.5 °C/km). Note that this approach does not rely on the actual closure temperatures for each method, only the relative differences (e.g., Reiners et al., 2003).

The TAM define the edge of the West Antarctic rift system. Rift systems are well known for having elevated heat flow during rifting with subsequent thermal relaxation after rifting (e.g., Houseman and England, 1986). Transient thermal effects associated with rifting may therefore have modified the local thermal regime in the Ferrar Glacier region. If so, what effect would this have on the interpretation of data and the use of the composite profile? Just offshore the TAM in McMurdo Sound (Fig. 1), the oldest rift-related sediments yet cored are ca. 34 Ma (Florindo et al., 2001) and unconformably overlie down-faulted Paleozoic basement. The oldest rift-related volcanics are ca. 25 Ma, also found in cores just offshore (McIntosh, 2000). While such a discussion is beyond the scope of this paper, rifting and subsidence of the Victoria Land Basin appears to have occurred later than the denudation recorded by the AFT and (U–Th)/He data and thus transient rift related effects are likely not significant. In addition, the consistent information from southern Victoria Land AFT age–elevation profiles, both close to the coast and further inland, covering the time period ca. 150–40 Ma (Gleadow and Fitzgerald, 1987; Fitzgerald, 1992) suggest that rift-related transient thermal effects have not noticeably effected the thermochronologic data set. We use 22.5 °C/km as the paleo-geothermal gradient based on earlier studies and also because this paleo-geothermal gradient represents a time of relatively tectonic and thermal stability (e.g., as demonstrated by the presence of an exhumed PAZ at Cathedral Rocks) just prior to when denudation began at ca. 50 Ma. The paleo-geothermal gradient is used to constrain the magnitude of denudation and hence the average denudation rates since ~50 Ma, but not to constrain apparent denudation rates based on the slope of the age–elevation profile. Those slope-derived apparent denudation rates will be an underestimate if the paleo-geothermal gradient increased since ~50 Ma, due to either advection (Mancktelow and Grasemann, 1997), although the effect of this appears minimal, or transient rift related effects, as discussed above.

In general, the best-fit lines through the (U–Th)/He weighted-mean ages (and by inference, the minimum (U–Th)/He lines) from Cathedral Rocks and Peak 1880 define similar *T–t* paths to those defined from AFT thermochronology (Fig. 11). The separation between the weighted mean line and the minimum (U–Th)/He line gives a qualitative measure of the cooling rate — if they are relatively far apart as for Cathedral Rocks (Fig. 11a) the cooling rate is less compared to when the lines are close together, as for Peak 1880 (Fig. 11b). At Cathedral Rocks the average AFT determined denudation rate 50–15 Ma is ≤125 m/m.y and the measured slope (apparent denudation rate) of the (U–Th)/He weighted means from ~50 to 40 Ma is 161 ± 63 m/m.y. (1σ). If we apply a topographic correction to the apatite (U–Th)/He apparent denudation rate by multiplying it by $(1-\alpha)$ if $\alpha = \sim 25\%$ (Section 2.3), the "topographically corrected denudation rate" is ~121 m/m.y. If we accept that the thermal modeling of this profile (Fig. 5) indicates that the onset of this rapid denudation was ~50 Ma: this implies that the dashed line [i] (Fig. 11a) is the most likely *T–t* path. Path [i] lies between the weighted mean (U–Th)/He ages and the minimum (U–Th)/He age line and agrees well with the AFT-determined cooling path. Thus, from the Cathedral Rocks profile (Fig. 11a) a very robust and simple interpretation of the data is slow cooling (<1 °C/m.y.) from the mid-Cretaceous to the

early Eocene followed by faster cooling (≤2.8 °C/m.y., denudation rate ≤125 m/m.y.). A more subtle interpretation is that there was a period of denudation recorded beginning in the mid-Cretaceous (onset ~95 Ma) although this is minor. We cannot further refine the post-early Eocene (since ~50 Ma) *T–t* path using the data we have, except to note that the new interpretation of the (U–Th)/He data is compatible with the AFT-derived cooling history.

At Peak 1880, the AFT constrained average denudation rate 40–15 Ma is ≤172 m/m.y., whereas the measured slope of the weighted mean (U–Th)/He ages for the samples below 800 m (i.e., those samples we have identified as having the cooled more rapidly) is 1114 ± 694 m/m.y. (1σ). If we apply a topographic correction to the apatite (U–Th)/He apparent denudation rate by multiplying it by $(1-\alpha)$, if $\alpha = \sim 25\%$ (Section 2.3), the "topographically corrected denudation rate" is $\sim 835 \pm 500$ m/m.y. Poorly constrained as it is, a denudation rate of this magnitude will likely modify the thermal structure of the upper crust and will slightly underestimate the true denudation rate (Mancktelow and Grasemann, 1997). While this apparently higher denudation rate is poorly constrained, a more rapid denudation rate is also implied by the reduced separation between the weighted mean (U–Th)/He line and the minimum (U–Th)/He line (i.e., the reduced variation in single grain (U–Th)/He ages). Its seems likely then that for the period covered by the steep part of the (U–Th)/He profile (i.e., the late Eocene), the denudation rate was greater than the average denudation rate determined by the AFT data and thus the cooling rate was also greater, likely >7 °C/m.y. and perhaps in excess of 20 °C/m.y.

The weighted mean (U–Th)/He line from Peak 1880 has an inflection indicating a slowing in the cooling (denudation) rate at ca. 47 Ma and then an increase at ca. 38 Ma. Our preferred cooling path (dashed line [i]; Fig. 11b) lies between the weighted mean (U–Th)/He line and the minimum (U–Th)/He line; thus, we would place the slowing of the cooling rate at ca. 43 Ma with an increase in rate at 35–37 Ma. Such refinements within the overall defined "best fit line" (thick grey line constrained by the AFT data), while necessarily being aware of the caveats involved, indicate that denudation was episodic, typical of TAM denudation as revealed in previous thermochronologic data (Stump and Fitzgerald, 1992) and also in the offshore record (e.g., Fielding et al., in review). Thus, from the Peak 1880 profile (Fig. 11b), a very robust and simple interpretation of the data is slow cooling (~1.9 °C/m.y.) accompanying slow denudation (~85 m/m.y.) from Late Cretaceous to early Eocene and then a slowing until the onset of major denudation in the late-middle Eocene (~40 Ma). A more subtle interpretation is that the Peak 1880 profile records denudation in the Late Cretaceous to early Eocene, a slowing in rate until denudation begins in the middle Eocene (ca. 43 Ma) and then perhaps a slight slowing until continuing in the late Eocene (~37–35 Ma).

If we construct our composite profiles using a higher paleo-geothermal gradient than the 22.5 °C/km used for Fig. 11, the AFT and (U–Th)/He data move closer together (vertically), making interpretation easier, and our interpretation remains unchanged. If we construct Fig. 11 using a lower paleo-geothermal gradient than 22.5 °C/km the AFT and (U–Th)/He data move further apart, there is less overlap of the (U–Th)/He trend lines with the AFT-derived cooling path and as a result implies a higher initial denudation rate before linking with the preferred (U–Th)/He path [i]. Using too low a paleo-geothermal gradient to construct this composite profile is contradictory, because as the AFT and (U–Th)/He data sets move further apart, a higher initial apparent denudation rate (based on the increased slope of the age–elevation profile) is required.

As mentioned in Section 2.3, we should conceivably be able to use the elevation difference between identical AFT and (U–Th)/He ages to determine a paleo-geothermal gradient, but the large variation in single grain (U–Th)/He ages precludes a realistic estimate. However, it is worthwhile undertaking this exercise using the weighted mean (U–Th)/He age-line, the minimum age-line and the preferred path, using an elevation for each where the respective lines intersect a certain age. Care must be taken that the time selected represents closure temperature age for both the AFT ages and the (U–Th)/He ages. In this example, we use 45 Ma. At 45 Ma, the AFT best-fit line elevations are ~300 m at Peak 1880 and 400 m at Cathedral Rocks. At Peak 1880, the 45 Ma elevation of the weighted mean (U–Th)/He age line is ~900 m, and the elevation of both the minimum (U–Th)/He age line and the preferred line [i] 1300 m. Using 30 °C as the difference in closure temperatures yields paleo-geothermal gradient estimates of ~50 °C/km (weighted mean line) and 23 °C/km (minimum age and preferred lines). Undertaking the same exercise at Cathedral Rocks yields paleo-geothermal gradient estimates of ~250 °C/km (weighted mean line), ~19 °C/km (minimum age line) and ~33 °C/km (preferred line [i]). The reasonable paleo-geothermal gradient estimates for our preferred cooling path at both profiles suggests that our approach to the interpretation of this data, i.e., that the "true" age lies between the weighted mean and the minimum age is correct.

5. Conclusions

A suite of samples collected from two vertical profiles along the Ferrar Glacier in southern Victoria Land, Antarctica exhibit considerable variation of single grain (U–Th)/He ages within individual samples. The cooling history of these samples is relatively well constrained by AFT thermochronology, and this allows us to relate variation of single grain ages with cooling rate. We also consider other mitigating factors (summarized in Table 3) to explain the variation of single grain ages. These factors include the presence of U- and Th-rich (micro)-inclusions, fluid inclusions, variation in crystal size, α-particle ejection correction, zonation and α-particle ejection correction, impediment of diffusion of ^{4}He from a crystal or implantation of ^{4}He from outside a crystal, plus any contribution of radiogenic helium from ^{147}Sm decay.

1. In this study, the intra-sample variation of (U–Th)/He single ages is dependent on cooling rate. When the cooling rate is relatively rapid, the variation of ages is minimized. When the rate of cooling is comparatively slower or samples are resident in a HePRZ prior to more rapid cooling, the variation of single grain ages can be considerable.
2. We exclude the presence of inclusions or variable grain size as the dominant reason for the variation in single grain ages. When outlier single grain ages due to the presence of inclusions are suspected, the criterion of Chauvenet provides an objective method to justify the exclusion of suspected outliers from a population.
3. The variation of single grain ages is due in part to the non-homogeneity of U and Th distribution within a grain, the resulting He-concentration profile and the correction for α-particle ejection (F_T correction factor) that assumes a uniform distribution of U and Th. If the grain has a higher [U,Th] core, especially if the majority of U and Th are ≥ 1 stopping distance from the grain boundary, then the number of α-particles retained are greater than expected and the F_T corrected age will therefore be greater than the "true age". If the grain has a high [U,Th] rim, especially if the majority of U and Th are ≤ 1 stopping distance from the grain boundary, then the number of α-particles retained are less than expected and the F_T corrected age will therefore be less than the "true age" (Fig. 8). Thus, if a number of grains are dated and the distribution of U and Th is non-uniform, then following the F_T correction, the grains will have a range of ages.
4. Slow cooling through, or residence within a HePRZ, accentuates the intra-sample variation of single grain ages. This is because diffusion modifies the concentration profile of ^{4}He, which is dependent on the initial distribution of parent U and Th within the grain, or may be modified by external α-particle implantation. If the cooling rate is rapid, little modification of the concentration profile takes place and the variation in single grain ages is only enhanced due to the effects of the F_T correction (that assumes a uniform U and Th distribution). If the rate of cooling is slow, the concentration profile produced by α-particle decay can be substantially modified and the differences in He-concentration profiles between rim-rich and rim-poor grains are accentuated. This effect, combined with the F_T correction (that assumes an uniform U and Th distribution), results in an even greater variation of intra-sample ages.
5. In cases where considerable variation in (U–Th)/He single grain ages exist, we suggest determining the weighted mean of the individual ages, once any outlier single grain (U–Th)/He ages are excluded, and then using that line to guide placement of a minimum (U–Th)/He line. The true age will lie between the minimum (U–Th)/He age line and the weighted mean age line.
6. The variation of single grain ages within an exhumed HePRZ should be systematic. The variation of ages near the base of a HePRZ will be small, as ^{4}He loss by diffusion is rapid and the dominant mechanism. Towards the middle of a HePRZ, as comparative loss via diffusion diminishes, the variation in single grain ages is maximized. Above the top of a HePRZ loss via α-particle ejection dominates.
7. A variation in the single grain age distributions should also be expected in zircon (U–Th)/He dating, titanite (U–Th)/He dating and any other minerals dated by the (U–Th)/He method when U and Th zoning occurs, and/or samples have been slowly cooled.
8. Combining the AFT and (U–Th)/He data along with thermal modeling and the new approach to interpreting significant variation of single grain (U–Th)/He ages, we were better able to constrain the *T–t* path and denudation histories derived from these two profiles. Overall, the two profiles reveal a similar history of episodic cooling (denudation): slow cooling in the Late Cretaceous and Early Cenozoic followed by an increased cooling rate in the early Eocene. In detail, the cooling (denudation) histories are subtly different. The Cathedral Rocks profile indicates slow cooling from the Cretaceous to the early Cenozoic but with a period of slightly faster cooling (denudation) begin-

ning ~95 Ma. At ~50 Ma, the rate of cooling (denudation) increased again. In contrast, cooling in the Late Cretaceous–early Eocene at Peak 1880 was more rapid than at Cathedral Rocks and continued until ca. 55 Ma. The major cooling (denudation) episode began in the mid-Eocene (~43 Ma) but appears to be episodic with a slowing in rate before continuing in the late Eocene (~37–35 Ma).

Acknowledgements

We thank Ken Farley for his advice and comments on an early version of this manuscript. We gratefully acknowledge the patience and skill of Lindsey Hedges. Tibor Dunai is thanked for providing us with the program DECOMP. Todd Ehlers and an anonymous reviewer are thanked for their constructive reviews that improved this manuscript. Fitzgerald and Baldwin acknowledge support from National Science Foundation Grants OPP-0002824 and OPP-9615294. These samples were originally collected as part of Antarctic fieldwork through the Antarctic Research Centre of Victoria University of Wellington. Samples were originally processed at the University of Melbourne with irradiation supported by the Australian Research Grants Scheme and the Australian Institute of Nuclear Science and Engineering. [**PD**]

References

Allibone, A.J., Cox, S.C., Graham, I.J., Smillie, R.W., Johnstone, R.D., Ellery, S.G., Palmer, K., 1993. Granitoids of the Dry Valleys area, southern Victoria Land, Antarctica: plutons, field relationships, and isotopic dating. New Zealand Journal of Geology and Geophysics 36, 281–297.

Armstrong, P.A., Ehlers, T.A., Chapman, D.S., Farley, K.A., Kamp, P.J.J., 2003. Exhumation of the central Wasatch Mountains, Utah: 1. Patterns and timing of exhumation deduced from low-temperature thermochronology data. Journal of Geophysical Research 108 (B3), 2173. doi:10.1029/2001JB001708.

Ballentine, C.J., Burnard, P.G., 2002. Production, release and transport of noble gases in the continental crust. In: Porcelli, D., Ballentine, C.J., Wieler, R. (Eds.), Noble Gases in Geochemistry and Cosmochemistry. Reviews in Mineralogy and Geochemistry. Mineralogical Society of America, Washington D.C., pp. 481–538.

Ballentine, C.J., Burgess, R., Marty, B., 2002. Tracing fluid origin, transport and interaction in the crust. In: Porcelli, D., Ballentine, C.J., Wieler, R. (Eds.), Noble Gases in Geochemistry and Cosmochemistry. Reviews in Mineralogy and Geochemistry. Mineralogical Society of America, Washington D.C., pp. 371–409.

Belton, D.X., Kohn, B.P., Gleadow, A.J.W., 2004a. Quantifying "excess helium": some of the issues and assumptions in combined (U–Th)/He and fission track analysis. In: Andressien, P. (Ed.), 10th International Fission track Dating Conference. Amsterdam, pp. 18.

Belton, D.X., Lorencak, M., Carter, T.J., Norman, M., Kohn, B.P., Gleadow, A.J.W., 2004b. Samarium in apatite: contributions to radiogenic helium and the effect on (U–Th)/He thermochronology. In: Andressien, P. (Ed.), 10th International Fission track Dating Conference. Amsterdam, pp. 40.

Brandon, M.T., Roden-Tice, M.K., Garver, J.I., 1998. Late Cenozoic exhumation of the Cascadia accretionary wedge in the Olympic Mountains, northwest Washington State. Geological Society of America Bulletin 110 (8), 985–1009.

Braun, J., 2002a. Estimating exhumation rate and relief evolution by spectral analysis of age–elevation datasets. Terra Nova 14, 210–214.

Braun, J., 2002b. Quantifying the effect of recent relief changes on age–elevation relationships. Earth and Planetary Science Letters 200, 331–343.

Brown, R.W., 1991. Backstacking apatite fission-track "stratigraphy": a method for resolving the erosional and isostatic rebound components of tectonic uplift histories. Geology 19, 74–77.

Brown, R.W., Summerfield, M.A., 1997. Some uncertainties in the derivation of rates of denudation from thermochronologic data. Earth Surface Processes and Landforms 22, 239–248.

Brown, R.W., Summerfield, M.A., Gleadow, A.J.W., 1994. Apatite fission track analysis: its potential for the estimation of denudation rates and implications for models of long-term landscape development. In: Kirby, M.J. (Ed.), Process Models and Theoretical Geomorphology. John Wiley and Sons Ltd.

Burtner, R.L., Nigrini, A., Donelick, R.A., 1994. Thermochronology of Lower Cretaceous source rocks in the Idaho–Wyoming thrust belt. American Association of Petroleum Geologists Bulletin 78 (10), 1613–1636.

Calkin, P.E., 1974. Subglacial geomorphology surrounding the ice-free valleys of southern Victoria Land. Journal of Glaciology 13 (69), 415–429.

Carlson, W.D., Donelick, R.A., Ketcham, R.A., 1999. Variability of apatite fission-track annealing kinetics: I. Experimental results. American Mineralogist 84, 1213–1223.

Crowhurst, P.V., Green, P.F., Farley, K.A., Jacobs, J., Griffin, B.J., 2004. 'Anomalously old' He ages: what causes them and what can we do about them? In: Andressien, P. (Ed.), 10th International Fission track Dating Conference. Amsterdam, pp. 19.

Deino, A., Potts, R., 1990. Single crystal $^{40}Ar/^{39}Ar$ dating of the Olorgesailie Formation, Southern Kenya Rift. Journal of Geophysical Research 95 (B6), 8453–8470.

Dodson, M.H., 1973. Closure temperatures in cooling geochronological and petrological systems. Contributions to Mineralogy and Petrology 40, 259–274.

Donelick, R.A., 1991. Crystallographic orientation dependence of mean etchable track length in apatite: a physical model and experimental observations. American Mineralogist 76, 83–91.

Donelick, R.A., Ketcham, R.A., Carlson, W.D., 1999. Variability of apatite fission track annealing kinetics: II. Crystallographic orientation effects. American Mineralogist 84, 1224–1234.

Dunai, T.J., Porcelli, D., 2002. Storage and transport of noble gases in the subcontinental lithosphere. In: Porcelli, D., Ballentine, C.J., Wieler, R. (Eds.), Noble Gases in Geochemistry and Cosmochemistry, Reviews in Mineralogy and Geochemistry. Mineralogical Society of America, Washington D.C., pp. 371–409.

Ehlers, T.A., Farley, K.A., 2003. Apatite (U–Th)/He thermochronometry: methods and applications to problems in tectonic and surface processes. Earth and Planetary Science Letters 206, 1–14.

Ehlers, T.A., P.A., A., Chapman, D.S., 2001. Normal fault thermal regimes and the interpretation of low-temperature thermochronometers. Physics of the Earth and Planetary Interiors 126, 179–194.

Ehlers, T.A., Willett, S.D., Armstrong, P.A., Chapman, D.S., 2003. Exhumation of the central Wasatch Mountains, Utah: 2. Thermokinematic model of exhumation, erosion, and thermochronometer interpretation. Journal of Geophysical Research 108 (B3), 2173. doi:10.1029/2001JB001723.

Elliot, D.H., Fleming, T.H., 2004. Occurrence and dispersal of magmas in the Jurassic Ferrar large igneous province, Antarctica. Gondwana Research 7 (1), 223–237.

Farley, K.A., 2000. Helium diffusion from apatite: general behaviour as illustrated by Durango fluorapatite. Journal of Geophysical Research 105, 2903–2914.

Farley, K.A., 2002. (U–Th)/He dating: techniques, calibrations, and applications. In: Porcelli, D., Ballentine, C.J., Wieler, R. (Eds.), Noble Gases in Geochemistry and Cosmochemistry, Reviews in Mineralogy and Petrology. Mineralogical Society of America, Washington D.C., pp. 819–844.

Farley, K.A., Wolf, R.A., Silver, L.T., 1996. The effects of long alpha-stopping distances on (U–Th)/He ages. Geochimica et Cosmochimica Acta 60 (21), 4223–4229.

Faure, G., 1986. Principles of Isotope Geology. Wiley, New York. 589 pp.

Fielding, C.R., Henrys, S.A. and Wilson, T.J., in review. Rift history of the western Victoria Land Basin: A new perspective based on integration of cores with seismic reflection data. In: D. Futterer (Ed.), Antarctic contributions to Global earth Science. Springer-Verlag, Berlin.

Fitzgerald, P.G., 1992. The Transantarctic Mountains of southern Victoria Land: the application of apatite fission track analysis to a rift shoulder uplift. Tectonics 11, 634–662.

Fitzgerald, P.G., 1994. Thermochronologic constraints on post-Paleozoic tectonic evolution of the central Transantarctic Mountains, Antarctica. Tectonics 13, 818–836.

Fitzgerald, P.G., 2002. Tectonics and landscape evolution of the Antarctic plate since Gondwana breakup, with an emphasis on the West Antarctic rift system and the Transantarctic Mountains. In: Gamble, J.A., Skinner, D.N.B., Henrys, S. (Eds.), Antarctica at the Close of a Millennium. Proceedings of the 8th International Symposium on Antarctic Earth Science, The Royal Society of New Zealand Bulletin. Royal Society of New Zealand, pp. 453–469.

Fitzgerald, P.G., Gleadow, A.J.W., 1990. New approaches in fission track geochronology as a tectonic tool: examples from the Transantarctic Mountains. Nuclear Tracks 17, 351–357.

Fitzgerald, P.G., Sandiford, M., Barrett, P.J., Gleadow, A.J.W., 1986. Asymmetric extension associated with uplift and subsidence in the Transantarctic Mountains and Ross Embayment. Earth and Planetary Science Letters 81, 67–78.

Fitzgerald, P.G., Sorkhabi, R.B., Redfield, T.F., Stump, E., 1995. Uplift and denudation of the central Alaska Range: a case study in the use of apatite fission-track thermochronology to determine absolute uplift parameters. Journal of Geophysical Research 100, 20175–20191.

Florindo, F., Wilson, G.S., Roberts, A.P., Sagnotti, L., Verosub, K.L., 2001. Magnetostratigraphy of late Eocene–early Oligocene strata from the CRP-3 core, Victoria Land Basin, Antarctica. Terra Antartica 8 (3), 599–613.

Francis, J.E., 1999. Evidence from fossil plants for Antarctic Palaeoclimates over the past 100 million year. In: Barett, P.J., Orombelli, G. (Eds.), Geological Records of Global and Planetary Changes. Terra Antartica Reports, Siena, pp. 43–52.

Galbraith, R.F., 1981. On statistical models for fission track counts. Journal of the International Association of Mathematical Geologists 13, 471–488.

Galbraith, R.F., Laslett, G.M., 1993. Statistical models for mixed fission track ages. Nuclear Tracks and Radiation Measurements 21, 459–470.

Gallagher, K., 1995. Evolving temperature histories from apatite fission-track data. Earth and Planetary Science Letters 136, 421–435.

Gallagher, K., Brown, R.W., Johnson, C., 1998. Fission track analysis and its application to geological problems. Annual Review of Earth and Planetary Science Letters 26, 519–572.

Gleadow, A.J.W., Duddy, I.R., 1981. A natural long term annealing experiment for apatite. Nuclear Tracks and Radiation Measurements 5, 169–174.

Gleadow, A.J.W., Fitzgerald, P.G., 1987. Uplift history and structure of the Transantarctic Mountains: new evidence from fission track dating of basement apatites in the Dry Valleys area, southern Victoria Land. Earth and Planetary Science Letters 82, 1–14.

Gleadow, A.J.W., Duddy, I.R., P.F., G., Lovering, J.F., 1986. Confined fission track lengths in apatite — a diagnostic tool for thermal history analysis. Contributions to Mineralogy and Petrology 94, 405–415.

Green, P.F., 1981. A new look at statistics in fission track dating. Nuclear Tracks and Radiation Measurements 5, 77–86.

Green, P.F., 1985. Comparison of zeta calibration baselines for fission-track dating of apatite, zircon and sphene. Chemical Geology (Isotope Geoscience Section) 58, 1–22.

Green, P.F., Duddy, I.R., Gleadow, A.J.W., Tingate, P.T., Laslett, G.M., 1986. Thermal annealing of fission tracks in apatite: 1. A qualitative description. Isotope Geoscience 59, 237–253.

Hendriks, B.W.H., Redfield, T.F., 2005. Apatite fission track and (U–Th)/He data from Fennoscandia: an example of underestimation of fission track annealing in apatite. Earth and Planetary Science Letters 236, 443–458.

Hourigan, J.K., Reiners, P.W., Brandon, M.T., 2005. U–Th zonation-dependent alpha-ejection in (U–Th)/He chronometry. Geochimica et Cosmochimica Acta 69 (13), 3349–3365.

House, M.A., Wernicke, B.P., Farley, K.A., Dumitru, T.A., 1997. Cenozoic thermal evolution of the central Sierra Nevada, California, from (U–Th)/He thermochronometry. Earth and Planetary Science Letters 151, 167–179.

House, M.A., Wernicke, B.P., Farley, K.A., 1998. Dating topography of the Sierra Nevada, California, using (U–Th)/He ages. Nature 396, 66–69.

House, M.A., Farley, K.A., Kohn, B.P., 1999. An empirical test of helium diffusion in apatite: borehole data from the Otway Basin, Australia. Earth and Planetary Science Letters 170, 463–474.

House, M.A., Wernicke, B.P., Farley, K.A., 2001. Paleo-geomorphology of the Sierra Nevada, California, from (U–Th)/He ages in apatite. American Journal of Science 301, 77–102.

Houseman, G., England, P., 1986. A dynamical model of lithospheric extension and sedimentary basin formation. Journal of Geophysical Research 91 (B1), 719–729.

Hurford, A.J., Green, P.F., 1983. The zeta age calibration of fission track dating. Isotope Geoscience 1, 285–317.

Kelley, S., 2002. K–Ar and Ar–Ar dating. In: Porcelli, D., Ballentine, C.J., Wieler, R. (Eds.), Noble Gases in Geochemistry and Cosmochemistry, Reviews in Mineralogy and Geochemistry. Mineralogical Society of America, Washington D.C., pp. 785–818.

Ketcham, R.A., Donelick, R.A., Carlson, W.D., 1999. Variability of apatite fission track annealing kinetics: III. Extrapolation to geological time scales. American Mineralogist 84, 1235–1255.

Ketcham, R.A., Donelick, R.A., Donelick, M.B., 2000. AFTSolve: a program for multi-kinetic modeling of apatite fission-track data. Geological Materials Research 2, 1–32.

Laslett, G.M., Gleadow, A.J.W., Duddy, I.R., 1984. The relationship between fission track length and density in apatite. Nuclear Tracks and Radiation Measurements 9, 29–38.

Lippolt, H.J., Leitz, M., Wernicke, R.S., Hagedorn, B., 1994. (Uranium+thorium)/helium dating of apatite: experience with samples from different geochemical environments. Chemical Geology; Isotope Geoscience 112, 179–191.

Lister, G.S., Baldwin, S.L., 1996. Modeling the effect of arbitrary *P–T–t* histories on argon diffusion in minerals using the MacArgon program for the Apple Macintosh. Tectonophysics 253, 83–109.

Long, A., Rippeteau, B., 1974. Testing contemporaneity and averaging radiocarbon dates. American Antiquity 39 (2), 205–215.

Lovera, O.M., Richter, F.M., Harrison, T.M., 1989. The $^{40}Ar/^{39}Ar$ thermochrometry for slowly cooled samples having a distribution of diffusion domain sizes. Journal of Geophysical Research 94, 17917–17935.

Mancktelow, N.S., Grasemann, B., 1997. Time-dependent effects of heat advection and topography on cooling histories during erosion. Tectonophysics 270, 167–195.

Marchant, D.R., Swisher, C.C., Lux, D.R., West, D.P., Denton, G.H., 1993. Pliocene paleoclimate and East Antarctic Ice-Sheet history from surficial ash deposits. Science 260, 667–670.

Marchant, D.R., Denton, G.H., Swisher, C.C., Potter, N., 1996. Late Cenozoic Antarctic paleoclimate reconstructed from volcanic ashes in the Dry Valleys region of southern Victoria Land. Geological Society of America Bulletin 108, 181–194.

McIntosh, W.C., 2000. $^{40}Ar/^{39}Ar$ geochronology of tephra and volcanic clasts in CRP-2A, Victoria Land Basin, Antarctica. Terra Antartica 7 (4), 621–630.

Meesters, A.G.C.A., Dunai, T.J., 2002a. Solving the production–diffusion equation for finite diffusion domains of various shapes: Part I. Implications for low-temperature (U–Th)/He thermochronology. Chemical Geology 186, 333–344.

Meesters, A.G.C.A., Dunai, T.J., 2002b. Solving the production–diffusion equation for finite diffusion domains of various shapes: Part II. Application to cases with α-ejection and non-homogeneous distribution of the source. Chemical Geology 186, 347–363.

Mitchell, S.G., Reiners, P.W., 2003. Influence of wildfire on apatite and zircon (U–Th)/He ages. Geology 31, 1025–1028.

O'Sullivan, P.B., Parrish, R.R., 1995. The importance of apatite composition and single-grain ages when interpreting fission track data from plutonic rocks: a case study from the Coast Ranges, British Columbia. Earth and Planetary Science Letters 132, 213–224.

Potts, P.J., 1987. A Handbook of Silicate Rock Analysis. Chapman and Hall, New York. 622 pp.

Reiners, P.W., Farley, K.A., 2001. Influence of crystal size on apatite (U–Th)/He thermochronology: an example from the Bighorn Mountains, Wyoming. Earth and Planetary Science Letters 188, 413–420.

Reiners, P.W., Zhou, Z., Ehlers, T.A., Changhai, X., Brandon, M.T., Donelick, R.A., Nicolescu, S., 2003. Post-progenic evolution of the Dabie Shan, eastern China, from (U–Th)/He and fission track thermochronology. American Journal of Science 303, 489–518.

Shuster, D.L., Farley, K.A., 2003. $^{4}He/^{3}He$ thermochronometry. Earth and Planetary Science Letters 217, 1–17.

Shuster, D.L., Farley, K.A., Sisterton, J.M., Burnett, D.S., 2003. Thermochronometry quantifying the diffusion kinetics and spatial distributions of radiogenic ^{4}He in minerals containing proton-induced ^{3}He. Earth and Planetary Science Letters 217, 19–32.

Spell, T.L., McDougall, I., Doulgeris, A.P., 1996. Cerro Toledo Rhyolite, Lemez Volcanic Field, New Mexico: $^{40}Ar/^{39}Ar$ geochronology of eruptions between two caldera-forming events. Bulletin of the Geological Society of America 108 (12), 1549–1566.

Spencer, A.S., Kohn, B.P., Gleadow, A.J.W., Norman, M., Belton, D.X., Carter, T.J., 2004. The importance of residing in a good neighbourhood: rechecking the rules of the game for apatite (U–Th)/He thermochronology. In: Andressien, P. (Ed.), 10th International Fission track Dating Conference. Amsterdam, pp. 20.

Stockli, D.F., Farley, K.A., Dumitru, T.A., 2000. Calibration of the apatite (U–Th)/He thermochronometer on an exhumed fault block, White Mountains, California. Geology 28, 983–986.

Stockli, D.F., Dumitru, T.A., McWilliams, M.O., Farley, K.A., 2003. Cenozoic tectonic evolution of the White Mountains, California and Nevada. Geological Society of America Bulletin 115, 788–816.

Stump, E., Fitzgerald, P.G., 1992. Episodic uplift of the Transantarctic Mountains. Geology 20, 161–164.

Stüwe, K., Hintermüller, M., 2000. Topography and isotherms revisited: the influence of laterally migrating drainage divides. Earth and Planetary Science Letters 184, 287–303.

Stüwe, K., White, L., Brown, R., 1994. The influence of eroding topography on steady-state isotherms: application to fission track analysis. Earth and Planetary Science Letters 124, 63–74.

Sugden, D.E., Denton, D.H., Marchant, D.R., 1995. Landscape evolution of the Dry Valleys, Transantarctic Mountains: tectonic implications. Journal of Geophysical Research 100, 9949–9967.

Sugden, D.E., Marchant Jr., D.R., Souchez, N.P., Denton, R.A., Swisher, G.H., Tison, C.C., 1995. Preservation of Miocene glacier ice in East Antarctica. Nature 376, 412–414.

Summerfield, M.A., Stuart, F.M., Cockburn, H.A.P., Sugden, D.E., Denton, G.H., Dunai, T., Marchant, D.R., 1999. Long-term rates of denudation in the Dry Valleys, Transantarctic Mountains, southern Victoria Land, Antarctica based on in situ-produced cosmogenic ^{21}Ne. Geomorphology 27 (1–2), 113–129.

Tessensohn, F., Wörner, G., 1991. The Ross Sea rift system, Antarctica: structure, evolution, and analogues. In: Thompson, M.R.A., Crame, J.A., Thomson, J.W. (Eds.), Geological Evolution of Antarctica. Cambridge University Press, New York, pp. 273–277.

Warnock, A.C., Zeitler, P.K., Wolf, R.A., Bergman, S.C., 1997. An evaluation of low-temperature apatite U–Th/He thermochronometry. Geochimica et Cosmochimica Acta 61, 5371–5377.

Wilch, T.I., Lux, D.R., Denton, G.H., McIntosh, W.C., 1993. Minimal Pliocene–Pleistocene uplift of the Dry Valleys sector of the Transantarctic Mountains: a key parameter in ice-sheet reconstructions. Geology 21, 841–844.

Wilson, T.J., 1999. Cenozoic structural segmentation of the Transantarctic Mountains rift flank in southern Victoria Land. Global and Planetary Change 23, 105–127.

Wilson, G.S., Roberts, A.P., Verosub, K.L., Florindo, F., Sagnotti, L., 1998. Magnetobiostratigraphic chronology of the Eocene–Oligocene transition in the CIROS-1 core, Victoria Land margin, Antarctica: implications for Antarctic glacial history. Geological Society of America Bulletin 110, 35–47.

Wolf, R.A., Farley, K.A., Silver, L.T., 1996. Helium diffusion and low-temperature thermochronology of apatite. Geochimica et Cosmochimica Acta 60 (21), 4231–4240.

Zeitler, P.K., Herzig, A.L., McDougall, I., Honda, M., 1987. U–Th–He dating of apatite: a potential thermochronometer. Geochimica et Cosmochimica Acta 51, 2865–2868.